

Application of fuzzy *c*-means clustering for analysis of chemical ionization mass spectra: insights into the gas-phase chemistry of NO₃-initiated oxidation of isoprene

Rongrong Wu¹, Sören R. Zorn¹, Sungah Kang¹, Astrid Kiendler-Scharr^{1†}, Andreas Wahner¹
5 and Thomas F. Mentel^{1*}

¹Institute of Energy and Climate Research, Troposphere (IEK-8), Forschungszentrum Jülich GmbH, 52428 Jülich, Germany

† Deceased February-06th, 2023

10 *Correspondence to: Thomas F. Mentel (t.mentel@fz-juelich.de)

Abstract

Oxidation of volatile organic compounds (VOCs) can lead to the formation of secondary organic aerosol, a significant component of atmospheric fine particles, which can affect air quality, human health, and climate change. However, current understanding of the formation mechanism of SOA is still incomplete, which is not only due to the complexity of the chemistry, but also relates to analytical challenges in SOA precursor detection and quantification. Recent instrumental advances, especially the developments of high-resolution time-of-flight chemical ionization mass spectrometry (CIMS), greatly improved both detection and quantification of low- and extremely low-volatility organic molecules (L/ELVOCs), which largely facilitated the investigation of SOA formation pathways. However, analyzing and interpreting complex mass spectrometric data remains a challenging task. This necessitates the use of dimension-reduction techniques to simplify mass spectrometric data with the purpose of extracting chemical and kinetic information of the investigated system. Here we present an approach to apply fuzzy *c*-means clustering (FCM) to analyze CIMS data from a chamber experiment, aiming to investigate the gas-phase chemistry of nitrate radical initiated oxidation of isoprene.

15
20
25

The performance of FCM was evaluated and validated. By applying FCM to measurements, various oxidation products were classified into different groups based on their chemical and kinetic properties, and the common patterns of their time series were identified, which gave insights into the chemistry of the investigated system. The chemical properties of

30

clusters are described by elemental ratios and average carbon oxidation state, and the kinetic behaviors are parameterized with generation number and effective rate coefficient (describing the average reactivity of a species) by using the gamma kinetic parameterization model. In addition, the fuzziness of FCM algorithm provides a possibility to separate isomers or different chemical processes species are involved in, which could be useful for mechanism development. Overall FCM is a well applicable technique to simplify complex mass spectrometric data, and the chemical and kinetic properties derived from clustering can be utilized to understand the reaction system of interest.

1. Introduction

45 Volatile organic compounds (VOCs) in the atmosphere are oxidized by reactions with hydroxyl radicals (OH), ozone (O₃), nitrate radicals (NO₃), or Cl atoms, leading to the formation of condensable vapors such as low- and extremely low-volatility organic compounds (LVOCs/ ELVOCs) that subsequently condense onto existing particles or even form new particles, and thereby form secondary organic aerosol (SOA) (Donahue et al., 2012; Hallquist et al., 2009; Ziemann and Atkinson, 2012). SOA comprises a major fraction of the atmospheric submicron particulate matter and can have an adverse impact on air quality, human health, and climate (Hallquist et al., 2009; Jimenez et al., 2009; Pöschl, 2005; Spracklen et al., 2011; Zhang et al., 2007). Despite extensive studies on characterization of the products and mechanisms involved in VOC oxidation and SOA formation, how VOCs contribute to SOA formation is not yet fully understood. This is not only hampered by the complexity of the chemistry itself, but also by the remaining analytical challenges in detection of organic precursors with low volatility (Bianchi et al., 2019; Shrivastava et al., 55 2017).

Recent instrumental developments, especially the availability of high-resolution time-of-flight chemical ionization mass spectrometry (CIMS) in atmospheric research, made the direct detection of low-volatility vapors possible (Ehn et al., 2012; Ehn et al., 2014; Jokinen et al., 2015). Benefitting from this, it has been discovered that the highly oxygenated organic molecules (HOM), which are formed through a rapid gas-phase process called autooxidation and generally have very low volatilities, significantly contribute to SOA and even new particle formation (Crouse et al., 2013; Ehn et al., 2012; Ehn et al., 2014; Kirkby et al., 2016; Prasse et al., 2018). 60

While advanced mass spectrometers greatly enhance our capability to detect and quantify HOM and facilitate the investigation of HOM formation mechanism, the highly complex mass spectrometric data, which consists of hundreds to thousands of variables (i.e., detected ions) over thousands of points in time, makes the data processing and interpretation challenging. In addition, the mass spectrometers are unable to detect structures of molecules despite modern instruments with high resolution (e.g., over 10,000 m/Δm) (Breitenlechner et al., 2017; Krechmer et al., 2018), which significantly hinders the understanding of the involved chemical processes. Furthermore, it is difficult to refine and extract kinetic and mechanistic information directly from the mass spectrometric data. 70

To reduce the complexity of data analysis, dimension-reduction techniques are necessary, which compress various variables in a dataset into a few to a dozen of factors/
75 clusters based on the underlying correlation/ similarity of different variables, e.g., in terms of their sources or physicochemical properties, while retain the major chemical and kinetic information of investigated systems, and thus make the data analysis easier and more effective (Äijälä et al., 2017; Buchholz et al., 2020; Koss et al., 2020; Yan et al., 2016; Zhang et al., 2019).

80 Factorization is one of the major dimension-reduction techniques, within which positive matrix factorization (PMF) (Paatero, 1997; Paatero and Tapper, 1994) is the most commonly used approach in atmospheric science, especially for ambient measurements of particulate matter by aerosol mass spectrometer (Canonaco et al., 2013; Lanz et al., 2007; Lanz et al., 2008; Zhang et al., 2005; Zhang et al., 2011), as well as for VOC measurements in both field
85 and laboratory studies (Brown et al., 2007; Lanz et al., 2009; Li et al., 2021; Rosati et al., 2019; Vlasenko et al., 2009; Yuan et al., 2012). Principal component analysis (PCA) (Wold et al., 1987) is also a frequently used multivariate factor analysis technique for deconvolution and interpretation of gas- and particle-phase composition data (Sofowote et al., 2008; Wyche et al., 2015; Zhang et al., 2005). Additionally, non-negative matrix factorization (NMF),
90 which is very similar to the PMF approach, has been widely used in interdisciplinary fields (Devarajan, 2008; Fu et al., 2019; Lee and Seung, 1999), as well as in atmospheric science (Chen et al., 2013; Karl et al., 2018; Malley et al., 2014; Song et al., 2021). Despite the similarities in mathematical formulation and constraints to PMF, the NMF algorithm does not need an error matrix as input. This eliminates the potential impact of error estimation on
95 outcomes and makes it more user-friendly.

In addition to factorization methods, an increasing number of recent studies have employed clustering techniques to mass spectra data (Äijälä et al., 2017; Koss et al., 2020; Li et al., 2020; Priestley et al., 2021). For example, Äijälä et al. (2017) combined a clustering algorithm, *k*-means ++, with PMF to classify and characterize the organic component of air
100 pollution plumes detected by AMS. Li et al. (2020) developed a clustering algorithm named noise-sorted scanning clustering, based on the traditional density-based special clustering of applications combined with a noise algorithm, and thereafter applied this method to distinguish different types of thermal properties of various biogenic SOA. Koss et al. (2020) compared the performance of hierarchical clustering analysis (HCA) with PMF and gamma
105 kinetics parameterization in analyzing complex mass spectrometric data. Their results demonstrate the feasibility of HCA to identify major types of ions and patterns of time

behavior and to draw out bulk chemical properties of the system that can be useful for modeling. In addition, in a recent work by Priestley et al. (2021), HCA was applied to infer CHON functionality of products formed from benzene oxidation.

110 In this work, we choose the fuzzy *c*-means clustering algorithm (FCM) as the major technique to analyze CIMS data collected from a chamber experiment, aiming to investigate the gas-phase chemistry of the isoprene-NO₃ oxidation system. Isoprene is the most abundant BVOC on earth, and is highly reactive in the atmosphere, which is an important precursor of O₃ and SOA and thus imposes detrimental effects on climate and health (Carlton et al., 2009; 115 Surratt et al., 2019). The reaction of isoprene with NO₃ is an important source of SOA, but its gas-phase reaction mechanism, especially the multi-generation chemistry and the contribution of the corresponding oxidation products to SOA formation remain ambiguous so far (Carlton et al., 2009; Fry et al., 2018; Ng et al., 2008; Rollins et al., 2009; Wu et al., 2021). Fuzzy *c*-means clustering is the most widely used fuzzy clustering algorithm and is adopted in this 120 study considering the following three aspects. Firstly, FCM allows variables to be affiliated with multiple clusters, similar to factorization methods like PMF, NMF, and PCA. Conversely, hard clustering methods, such as the most popular *k*-means clustering, assign each variable exclusively into one cluster. In atmospheric chemistry, one compound can originate from several different sources, or a species detected may consist of isomers 125 produced from different chemical processes. Therefore, from this perspective, assigning a variable into multiple clusters with a quantified membership degree is more rational than assigning variables to mutually exclusive clusters. Secondly, FCM is more user-friendly since only the data matrix is needed as input, whereas additional information is required for factor analysis methods, such as the error matrix needed in PMF. Furthermore, receptor models like 130 PMF assume that the factor profiles remain constant over time and that the chemical species do not react with each other during the sampling period (Chen et al., 2011; Reff et al., 2007; Xie et al., 2022), which is not the case for chamber measurements.

By using FCM, variables with similar time behaviors will be grouped into the same cluster, and the centroid of the cluster (cluster center) can be used as a surrogate of these 135 variables. Therefore, the numerous species detected in a chemical system can be compressed to a much smaller number of clusters, each of which represents a typical chemical process/source with unique time behavior. By analyzing these cluster centers instead of the whole data set, one can obtain the chemical and kinetic properties of the investigated system in a much easier way. The significant reduction of the complexity of data analysis and the 140 chemical and kinetic information derived from this method can help to better understand the

chemical system of interest (Koss et al., 2020). In addition, to evaluate its performance, we applied FCM to a synthetic dataset derived from a box model with explicit mechanism. By exemplifying the functionality of such a clustering method in analyzing CIMS data, we propose that FCM is a useful method that offers a new approach to analyze mass spectrometric data and to derive useful information on chemical and kinetic properties of products that can help decipher the underlying reaction mechanism.

2. Methods

2.1 Data collection and processing

The experimental data used in this work were collected in the atmospheric simulation chamber SAPHIR at the Forschungszentrum Jülich, Germany, during the ISOPNO₃ campaign in 2018. The SAPHIR chamber is a double-walled Teflon (PEP) cylinder with an approximate volume of 270 m³ (5m in diameter, 20m in length). It is fixed by an aluminum frame with movable shutters that can be opened or closed to simulate daytime or nighttime chemistry. Trace gases in the chamber can be well mixed within 2 minutes with the help of two continuously operated fans. During an experiment, the chamber is filled with synthetic air and kept slightly over pressured (~ 35 Pa) to prevent permeation of outside air into the chamber. Due to small leakages and instrument sampling consumption, there is a replenishing flow into the chamber, which leads to a dilution rate of 4% – 7% h⁻¹. More details about the chamber setup and its performance can be found elsewhere (Rohrer et al., 2005).

The experiment selected here was conducted to characterize the gas-phase chemistry of NO₃-initiated oxidation of isoprene. O₃ and NO₂ were added in sequence to produce NO₃, followed by the addition of ~10 ppbv of isoprene to initiate the reaction. The injections were repeated four times (only NO₂ and O₃ were added in the last injection) to build up products and to facilitate later-generation oxidation. The mixing ratios of O₃ and NO₂ in the chamber were approximately 100 and 25 ppbv, respectively, after the first injection, as shown in Fig. S1. Detailed description of the experimental procedure can be found elsewhere (Wu et al., 2021).

During the campaign, a comprehensive set of instruments was deployed to measure radicals and closed-shell products in both gas- and particle phase, as described by Wu et al. (2021). In this work, however, we focus on the measurements acquired by a high-resolution time-of-flight chemical ionization mass spectrometer (Aerodyne Research Inc.) using Br⁻ as

reagent ion, which detected the HO₂ radical and the gas-phase products generated by the reaction of isoprene and NO₃. The mass spectrometer was operated in “V” mode with a mass resolution of 3000 – 4000 ($m/\Delta m$). A customized inlet was designed to connect the CIMS
175 directly to the chamber to reduce losses of the HO₂ radical and HOM in the sampling line (Albrecht et al., 2019). More information about settings and performance of the instrument can be found in our previous study (Wu et al., 2021).

The raw mass spectrometric data were processed using the Tofware toolkit (v. 2.5.11, Tofwerk AG/ Aerodyne Research Inc.) in Igor Pro (v.7.0.8, WaveMetrics) following the
180 routines described by Stark et al. (2015). High-resolution peak fitting was conducted in the mass range of m/z 60 – 600 to identify the chemical composition of detected ions. For high-resolution peak assignment, we fitted the observed peaks using predefined instrument functions (including peak shape, peak width as a function of m/z , and baseline). If necessary, contributions of more than one component were considered for the fit, in order to reduce the
185 residuals of the fitting. Once the peak numbers and peak positions were fixed, the chemical formula (consisting of C, H, O, and N atoms) of each peak was assigned manually by selecting from a formula list generated by the software. During the peak fitting, isotopes were constrained, and only plausible formulas with relative m/z deviations smaller than 10 ppm were considered. In addition, only molecule formulas with a time behavior commensurable
190 with expectations for the specific chemical system were assigned (Pullinen et al., 2020). For example, it is illogical if large amounts of organonitrates are observed under low NO_x conditions.

Overall, around 160 ions were identified by the Br⁻-CIMS. The background signal of each ion was determined from measurements prior to precursor injection and was subtracted
195 from the signal measured in the chamber. These ions consist of species related to real isoprene oxidation products, as well as other signals related to the ion source, internal standard, and interferences from chamber and tubing. The product ions are those produced by isoprene oxidation, and they should have visible changes (either increase or decrease) when the chemistry is initiated or modified. A simple way to select out the product ions from other
200 chemically irrelevant signals is to examine the time evolution of each ion. By comparing the signals before and after each injection, we can easily distinguish the product ions from others. Among all the identified ions, a total of 91 ions were recognized as product signals. Since we intend to investigate the underlying chemical relationships of different products through their time behavior, not the absolute concentration, normalized (to the sum of total ion counts)

205 signals were used for further analysis. Calibration procedures are described in more detail elsewhere (Wu et al., 2021).

In addition to abovementioned chamber data, we use a synthetic dataset from a box model with the default gas-phase reaction schemes of isoprene-NO₃ taken from the Master Chemical Mechanism (MCM) version 3.3.1 (Jenkin et al., 2015). For the modelling, 210 temperature, relative humidity, and dilution rate were constrained by using measured data. The initial concentrations of O₃, NO₂ and isoprene were added into the model according to the experimental schedule. Overall, the modelled concentrations of O₃, NO₂, NO₃ and isoprene match the measurements well (Fig. S2). The synthetic data was used to learn about the principal behaviors of time series (of products) in a complex chemical system with an 215 established complex mechanism. Detailed description of isoprene-NO₃ chemistry and evaluation of the model performance are outside the scope of this work. An updated mechanism for isoprene oxidation by NO₃ has been published recently by Carlsson et al. (2022).

2.2 Fuzzy *c*-means clustering (FCM)

220 Clustering is one of the major dimension-reduction techniques besides factorization, which groups a set of objects into a certain number of clusters according to their (dis)similarities, which are generally measured by a distance metric, such that objects within each cluster are much closer to each other than to those pertaining to other clusters (Hastie et al., 2009). The notion of a fuzzy set, first proposed by Zadeh (1965), gives an idea how to deal with data 225 with indistinct boundaries of clusters. Based on this concept, Bezdek et al. (1984) developed the fuzzy *c*-means clustering algorithm. In contrast to the hard clustering counterparts like *k*-means and *k*-medoids clustering, FCM allows each object to belong to multiple clusters with the membership degree measured by a value varying from 0 to 1 (Bezdek et al., 1984). Consequently, fuzzy clustering can better deal with non-discrete data, and thus is adopted 230 here to analyze CIMS data obtained from isoprene-NO₃ oxidation.

Fuzzy *c*-means clustering is one of the best-known fuzzy clustering algorithms by virtue of its simplicity, quick convergence, and wide applicability (Ghosh and Dubey, 2013; Ren et al., 2016; Yang, 1993;). It is a distance-based cluster assignment method, and its working principle is very similar to that of the *k*-means algorithm. FCM is conducted through an 235 iterative process which attempts to group all objects within a dataset into a predefined

number of clusters (c) with a degree of membership, and meanwhile minimize the sum of squared distance between the member objects and the cluster centroids, as defined in Eq. 1:

$$J_m(U, V) = \sum_{i=1}^c \sum_{j=1}^n u_{ij}^m d_{ij}^2 \quad (1)$$

where x_j is the object j in the dataset, u_{ij} is the membership degree of x_j to the i^{th} cluster, which is enforced to satisfy $u_{ij} \in [0, 1]$ and $\sum_{i=1}^c u_{ij} = 1$, d_{ij} denotes the distance between object x_j and the i^{th} cluster center v_i , and m is the fuzzifier ($m \in [1, \infty)$) that controls the fuzziness level of clustering.

Starting with an initial fuzzy partition matrix (U^0), either provided or randomly produced, the cluster centers (V) are calculated by

$$v_i = \frac{\sum_{j=1}^n u_{ij}^m \cdot x_j}{\sum_{j=1}^n u_{ij}^m} \quad (2)$$

for all i ($1 \leq i \leq c$) and afterwards the membership degrees of each object are updated by

$$u_{ij} = \left\{ \sum_{k=1}^c \left(\frac{d_{ij}}{d_{kj}} \right)^{\frac{2}{m-1}} \right\}^{-1} \quad (3)$$

The algorithm proceeds by repeating above process, and every iteration generates two new sets of V and U . The iteration ends when the algorithm converges (no significant change with further iteration, namely $\|U^{(t+1)} - U^{(t)}\| = \max_{i,j} \{|u_{ij}^{(t+1)} - u_{ij}^t|\} < \varepsilon$), or the predefined maximum number of iterations is reached. In this study, the FCM algorithm was implemented using the open-source scikit-fuzzy (v 0.4.2) package (<https://pypi.org/project/scikit-fuzzy/>) in Python.

2.3 Clustering parameters

As noted in Sect. 2.2, several parameters need to be specified ahead of executing FCM, including the number of clusters, the distance metric to measure (dis)similarity of objects, the value of the fuzzifier, the initial fuzzy partition matrix, the maximum number of iterations, and the stopping criterion. All these parameters can affect the partition outcomes, and among them the most important ones are the cluster number, the distance metric, and the fuzziness index. A brief introduction to these parameters and methods to determine their optimal values are given in the following sections.

2.3.1 Number of clusters (c)

Figuring out the optimal number of clusters (c) is one of the challenges in cluster analysis. The optimal number of clusters is related to the structure of the investigated dataset, and it has a critical impact on clustering outcomes. To our knowledge, none of the existing methods are feasible to determine the optimal cluster number in all possible cases and applications.

The frequently used method to address this problem is to set the search range of c , conducting clustering to generate solutions according to the predefined number of clusters, and then choosing one or several clustering validity indices (CVIs) to evaluate the outcomes. By comparing the values of CVI(s) of alternative clustering solutions obtained with different number of clusters, the appropriate c could be determined accordingly.

In this case, a validity index is used as a fitness function to evaluate the quality of the clustering results in terms of intra-cluster compactness and inter-cluster separation. In addition, CVIs play an extremely important role in automatically determining the appropriate number of clusters. Plenty of CVIs have been proposed in the past. Generally, these CVIs can be divided into three categories. The first type of CVIs only consider the property of membership degree in the calculation, such as the partition coefficient (Bezdek and Pal, 1998) and partition entropy (Simovici and Jaroszewicz, 2002), which are also the earliest validity indices for fuzzy clustering. The main disadvantage of such CVIs is that they lack direct connection to the geometry structure of the data. Considering this, another type of CVIs, such as Fukuyama-Sugeno index (Fukuyama, 1989), Xie-Beni index (Xie and Beni, 1991), Kwon index (Kwon, 1998) and Bouguessa-Wang-Sun index (Bouguessa et al., 2006), were proposed, which takes both membership degree and the geometry structure of data set into consideration. Given their advantages over those in the first category, we only chose CVIs belonging to the second category in this study. Different from the first two types of CVIs, the third type of CVIs makes use of the concept of hypervolume and density for evaluation. The fuzzy hypervolume and the average partition density (Gath and Geva, 1989) are the most popular two indices in this category. In this study, the second type of CVIs was chosen for the analysis considering its applicability to our data set.

Although there are various of CVIs, no CVI can always outperform others due to their own limitations and complexity of different datasets (Kryszczuk and Hurley, 2010; Wang et al., 2021). Generally, each CVI only attaches importance to a specific aspect or limited aspects of a clustering solution, while other aspects can be inadequately represented or even overlooked (Kryszczuk and Hurley, 2010). In order to overcome or at least diminish the

295 impact from this, we adopt multiple CVIs for the evaluation in this study. Among all the
alternatives, the following six CVIs were chosen, including the sum of within-cluster
variance (V_{SWCV} , Elbow method), Fukuyama-Sugeno index (V_{FS}), Xie-Beni index (V_{XB}),
Kwon index (V_{Kwon}), Bouguessa-Wang-Sun index (V_{BWS}) and fuzzy Silhouette (FS ,
Campello and Hruschka, 2006). They are the most frequently used CVIs in the literature and
300 are reported to perform well (Bouguessa and Wang, 2004; Campello and Hruschka, 2006;
Rawashdeh and Ralescu, 2012; Zhou et al., 2014). More information about these CVIs can be
found in Supplement S1.

With respect to the search range of c , a rule of thumb suggests that the maximum c
should not exceed \sqrt{n} (n here is the number of elements in a dataset) (Ren et al., 2016; Yu
305 and Cheng, 2002). Therefore, the search range of c could be set to $[2, \sqrt{n} + 1]$ in general. To
obtain a concrete result, for each c in this range, the FCM algorithm is performed 50 times
with the default settings ($m = 2$, metric = Euclidean distance, $\varepsilon = 1 \times 10^{-5}$). The selected CVIs
are calculated for each repetition, and the averages of results from 50 repetitions are used for
further analysis. By evaluating the variations in CVIs with different c , the expected optimal
310 number of clusters is determined.

2.3.2 Distance metric

The selection of an appropriate distance or (dis)similarity metric for clustering is also
challenging, since it not only relates to the inherent structure of the investigated data set, but
also depends on the analysis purpose. Various distance metrics have been proposed for
315 measuring the (dis)similarity between each pair of objects, among which the Euclidean
distance is the most frequently used metric. As defined by Eq. 4, the Euclidean distance
corresponds to the true geometrical distance between two objects. Most of the previous
studies adopted this metric by default for FCM (Haqiqi and Kurniawan, 2015; Nishom, 2019;
Singh et al., 2013). However, Euclidean distance may not always be appropriate. The
320 Euclidean distance assumes that each object is equally important during clustering, namely
the data being spherically distributed, so it is sensitive to outliers (Arora et al., 2019; Dik et
al., 2014). If the investigated data is not spherically distributed, using Euclidean distance
metric for clustering could potentially lead to unsatisfactory outcomes (Arora et al., 2019;
Gueorguieva et al., 2017; Vélez-Falconí et al., 2020).

$$325 \quad d(x, y) = \sqrt{\sum_{i=1}^n (x_i - y_i)^2} \quad (4)$$

where x and y are n -dimensional objects, with x_i and y_i denoting the i^{th} dimension of x and y , and \bar{x} and \bar{y} are the means of x and y in all dimensions, respectively.

In addition to Euclidean distance, other distance metrics, such as the Manhattan distance, the Eisen cosine distance, and the Pearson correlation distance, are used to measure (dis)similarity (Äijälä et al., 2017; Koss et al., 2020). The Manhattan distance is also named city block distance or taxicab distance. It computes the sum of the absolute differences between all sets of coordinates of pairwise objects following Eq. 5, which is reported to be less sensitive to noise (Dik et al., 2014). Another disadvantage of Manhattan distance is that the results would be different if the coordinate system is rotated (Vélez-Falconí et al., 2020). However, if the attributes are discrete or binary, the Manhattan distance is more effective than other metrics.

$$d(x, y) = \sum_{i=1}^n |x_i - y_i| \quad (5)$$

where x and y are n -dimensional objects, with x_i and y_i denoting the i^{th} dimension of x and y , and \bar{x} and \bar{y} are the means of x and y in all dimensions, respectively.

The Eisen cosine and the Pearson correlation distance are both correlation-based distance metrics. The Pearson correlation distance measures the linear dependence of two objects, while the cosine distance uses the cosine angle of two objects to measure their (dis)similarity. They are calculated by subtracting the correlation coefficient from 1, as defined by Eq. 6 and Eq. 7, and therefore they are invariant to the magnitudes of variables. Two objects are considered similar if they are highly correlated in terms of correlation-based distances, even though they may be far away from each other in Euclidean space. This is particularly beneficial when dealing with mass spectrometric data (mass profiles). The cosine distance is commonly used to measure the (dis)similarity of aerosol source profiles (Äijälä et al., 2017; Bozzetti et al., 2017; Heikkinen et al., 2021; Ulbrich et al., 2009). It should be noted that even though correlation-based metrics are called “distance”, strictly speaking, they are (dis)similarity metrics rather than distance metrics because they do not satisfy the triangle inequality anymore (Kaufman and Rousseeuw, 2009).

$$d(x, y) = 1 - \frac{|\sum_{i=1}^n x_i y_i|}{\sqrt{\sum_{i=1}^n x_i^2 \sum_{i=1}^n y_i^2}} \quad (6)$$

$$d(x, y) = 1 - \frac{\sum_{i=1}^n (x_i - \bar{x})(y_i - \bar{y})}{\sqrt{(\sum_{i=1}^n (x_i - \bar{x})^2) (\sum_{i=1}^n (y_i - \bar{y})^2)}} \quad (7)$$

355 where x and y are n -dimensional objects, with x_i and y_i denoti the i^{th} dimension of x and y ,
and \bar{x} and \bar{y} are the means of x and y in all dimensions, respectively.

Since the Euclidean distance can be severely affected by the scale of objects, which
means that the (dis)similarity between objects measured by Euclidean distance might get
skewed if input variables are in different scales or units. Therefore, it is highly recommended
360 to normalize the data before clustering, if Euclidean distance is chosen as a metric of
(dis)similarity. In this study, we intend to compare the time behaviors of different variables
directly, regardless of their differences in absolute intensity or detection sensitivity. Therefore,
we normalize the time-series data by using the Euclidean norm before clustering to eliminate
the effects of different branching ratios and sensitivity of species, and to facilitate the
365 comparison of different time patterns.

Since it is difficult to know the inherent structure of high-dimensional data, we also
make use of CVIs to figure out the suitable distance metric for FCM applied to our dataset.
By running FCM with four different distance metrics mentioned above and then calculating
the six CVIs accordingly while retaining all other parameters, we get four parallel results for
370 each CVI. The “optimal” distance metric is determined by comparing these outcomes. Again,
for each distance metric under scrutiny, the FCM algorithm was repeated 50 times to ensure
reliable outcomes. The averages of results from these runs are then utilized for subsequent
analysis.

2.3.3 Value of fuzzifier

375 The fuzzifier ($m, m \in [1, \infty)$) defines the fuzziness degree of the clustering. A proper value
of m can suppress the noise and smooth the membership function (Huang et al., 2012). When
 $m = 1$, FCM is equivalent to the k -means algorithm. The closer m is to 1, the crisper the
resulting solution becomes. On the contrary, as m becomes larger, the clustering outcomes
become fuzzier. When m approaches infinity, different cluster centers and the centroid of all
380 objects will coincide, and thereby all objects have the identical membership degree to each
cluster, namely $u_{ij} = 1/c$. Theoretically, the larger m is, the fuzzier the clustering outcomes
would be (Hammah and Curran, 1998). Therefore, m should be selected to fulfill the request
of maximum recognition of a partition with a fuzziness as small as possible.

According to previous studies, the optimal value of m varies in the range of 1 to 5
385 (Hathaway and Bezdek, 2001; Huang et al., 2012; Ozkan and Turksen, 2007; Pal and Bezdek,
1995; Wu, 2012), and it is often set to be 2, a default value recommended by Pal and Bezdek

(1995). However, it is reported that in many cases the true value of m deviates from this recommended value, which is believed to be biased by the data structure of interest (Huang et al., 2012; Hwang and Rhee, 2007; Schwämmle and Jensen, 2010; Yu et al., 2004; Zhou et al., 390 2014). A few methods have been proposed to determine the optimal value or range of the fuzzifier (Gao et al., 2000; Huang et al., 2012; Ozkan and Turksen, 2007; Schwämmle and Jensen, 2010). However, they are either empirical or only applicable for limited cases. It is still an open problem to determine the appropriate fuzzifier value in FCM.

In this study, we adopted the method proposed by Gao et al. (2000) to determine the 395 optimal fuzzifier value m^* . Based on their method, a fuzzy objective function (μ_G) and a fuzzy constraint function (μ_C) have been defined, and the intersection of μ_G and μ_C is supposed to be the value of m^* , as defined by Eq. 8:

$$m^* = \arg \left\{ \max_{\forall m} \{ \min \{ \mu_G(m), \mu_C(m) \} \} \right\} \quad (8)$$

Where μ_G is a fuzzy objective function, as calculated by Eq. 9:

$$400 \quad \mu_G(m) = \exp \left\{ -\alpha \times \frac{J_m(U,V)}{\max_{\forall m} (J_m(U,V))} \right\} \quad (9)$$

where α is a constant larger than 1, and generally set to be 1.5 in practice, and $J_m(U, V)$ is the objective function of fuzzy clustering as shown in Eq. 1.

And μ_C is a fuzzy constraint function as defined by

$$\mu_C(m) = \left\{ 1 + \beta \times \left(\frac{H_m(U,c)}{\max_{\forall m} (H_m(U,c))} \right) \right\}^{-1} \quad (10)$$

405 where β is a constant that is usually set to be 10 in practice, and $H_m(U, c)$ is the fuzzy partition entropy calculated by

$$H_m(U, c) = -\frac{1}{n} \sum_{i=1}^c \sum_{j=1}^n u_{ij} \cdot \log_a(u_{ij}) \quad (11)$$

where u_{ij} is the membership degree of object j to the i^{th} cluster, and a is a constant $\in (1, \infty)$ which is usually set to the mathematical constant.

410 Based on the fuzzy decision-making method, we search for m^* in the range of [1.1, 9] with an increment of 0.1. The number of clusters varies between 2 and 10, and the initial fuzzy partition matrix (U^0) is randomly created. Other parameters are fixed. For each setting, the algorithm is run 50 times for dependable results. By evaluating the variations of m^* with c and the initial values of membership degree, the optimal value of m is determined.

415 2.3.4 Other parameters and constraints

We find that when using a small number of iterations, FCM does not always return the same result for each run, and sometimes not even a valid solution. This is probably because the limit of iterations is reached before the algorithm converges. To avoid this, the maximum number of iterations was set to be 10000 in this study. In our case, however, hundreds of
420 iterations can already ensure a valid solution and reproducible results.

The initial fuzzy partition matrix was randomly created by the algorithm and 50 repetitions were used to evaluate the influence of U^0 on clustering outcomes. As for the stop criterion, the algorithm can offer reproducible results when this value is set to 1×10^{-3} or smaller. For the calculation of results selected for analysis in this study, the stop criterion was
425 set to 1×10^{-5} .

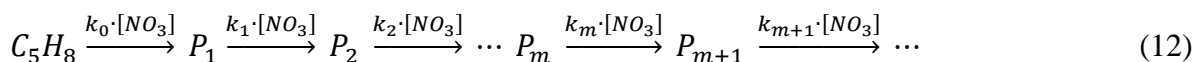
The clustering results of FCM are not as clear as that of k -means clustering, in which each object is forced to one cluster exclusively. Consequently, it is important to distinguish an invalid cluster and thereby to identify an invalid solution. According to the definition of the fuzzy clustering algorithm ($\sum_{i=1}^c u_{ij} = 1$), each object can only belong to one cluster with
430 a membership degree larger than 0.5. Therefore, we define a cluster with at least one object having the membership degree larger than 0.5 as a valid cluster, and a solution without any invalid clusters as a valid solution. In this work, only valid solutions were considered for further analysis.

2.4 Gamma kinetics parameterization (GKP)

435 The mass spectrometric data from chamber oxidation experiments not only contain chemical composition information of the products but also a great deal of kinetic clues. The kinetic information, mainly the reaction rate constant and the generation number (the oxidation steps needed to produce the target compound) underlying in the time series of each species, are useful for mechanism development. However, it is challenging to extract kinetic information
440 from time-series data, and there is only a limited number of studies which include determination of kinetic parameters based on gas-phase measurements (Koss et al., 2020; Zaytsev et al., 2019). In this study, we try to determine the kinetic parameters based on time-series data using the gamma kinetics parameterization (GKP). The GKP model describes the multistep reaction system as a linear system with first-order reactions, and it was originally
445 used in biological and chemical fields (Zhou and Zhuang, 2007). The model returns the so-called effective rate constant (overall rate of reactions in the pathway) and the generation

number that are implied by the time behaviors of individual species (Koss et al., 2020; Zhou and Zhuang, 2007). The GKP model was introduced for atmospheric chemistry studies by Koss et al. (2020) and has been successfully applied to parameterize the kinetics of gas-phase products formed from toluene and 1,2,4-trimethylbenzene oxidation in chamber studies (Koss
450 et al., 2020; Zaytsev et al., 2019).

According to the GKP method, the NO₃-initiated isoprene oxidation system can be described by Eq. 12:



455 where k_m is the rate constant of product P_m reacting with the NO₃ radical, and the subscript m denotes the number of oxidation steps (by NO₃) needed to form product P_m .

Typically, the rate constants for different reaction steps are disparate, and there is no simple analytical solution for the differential equations that describe Eq. 12. However, if assuming a single rate coefficient for all steps in a sequence, the differential equations in Eq.
460 12 become mathematically solvable. Additionally, the bimolecular reactions between P_m and NO₃ must be reduced to pseudo-first-order reactions by replacing the reaction time t with the integrated NO₃ exposure $\int_0^t [NO_3] dt$. The time series of P_m can then be described by Eq. 13 (Koss et al., 2020):

$$[X_m](t) = a(k[NO_3]\Delta t)^{m_G} e^{-k[NO_3]\Delta t} \quad (13)$$

465 where a is a scaling factor that relates to the product yield as well as to the instrument sensitivity (Koss et al., 2020), k is a second-order rate constant (cm³ molecule⁻¹ s⁻¹), and m_G is the generation number.

3. Results and discussion

3.1 Evaluation of clustering parameters

470 As mentioned earlier, one of the major hurdle in using FCM is the necessity to predefined several parameters. Inadequate selection of these parameters can result in unreasonable clustering outcomes. The number of clusters, the distance metric and the fuzziness value are the most important parameters that affect the partition. Therefore, in this section we will have a close look at these three parameters and evaluate their effects on the quality of clustering
475 based on the methods introduced in Sect. 2.3. The optimal values of these parameters are then determined for the analysis of our data.

3.1.1 Number of clusters (c)

To explore the effect of cluster number on partition results, we applied the FCM algorithm to the chamber data with c varying from 2 to 10. For each c in this range, the algorithm was run 50 times and the selected CVIs were calculated accordingly for each repetition. Despite some variations in specific CVIs among different repetitions, the trends of CVIs with changing cluster number and the optimal number of clusters indicated by each CVI are generally the same for each repetition.

Figure 1 depicts different CVIs as a function of number of clusters based on FCM results from 50 repetitions. For the sum of within-cluster variance (V_{SWCV}), the inflection point of the curve (so-called “elbow” point) indicates the best value of c , which is in our case 5 (Fig. 1a). The Fakuyama-Sugeno index (V_{FS}) uses the discrepancy between compactness and separation of clusters to measure the quality of a clustering solution (as defined by Eq. S2), and thus a smaller value of V_{FS} indicates a better partition (Fukuyama, 1989). In our case, the 8-cluster solution is the best option in terms of V_{FS} (Fig. 1b). Xie-Beni index (V_{XB}) is defined as the ratio of compactness and separation (Eq. S6), where the within-cluster compactness is measured by the sum of the within-cluster variance, while the between-cluster separation is measured by the minimum squared distance between cluster centers. Generally, the smaller V_{XB} is, the better a clustering solution can be, since under such conditions, objects within one cluster are much closer to each other but farther away to those in other clusters (Xie and Beni, 1991). According to Fig. 1c, $c = 2$ is the best option in terms of V_{XB} . However, when $c = 2$, the V_{SWCV} value is relatively large (Fig. 1a), which is not expected for a good clustering solution. When $c = 5$, the V_{XB} reaches a local minimum, and the V_{SWCV} curve also gets the maximum curvature at this point, indicating that the optimal cluster number might be 5 indeed. The Kwon index (V_{kwon}) is a modification of V_{XB} , which introduces a penalty function additionally to measure the cluster compactness together with the sum of within-cluster variance. As defined by Eq. S8, the penalty function measures the average squared distance between cluster centers and the overall mean of the dataset. By introducing this factor, V_{kwon} eliminates the monotonous decreasing tendency when c approaches the number of objects in the dataset (Kwon et al., 2021). Like V_{XB} , a smaller V_{kwon} indicates a better partition, and the results in Fig. 2d show that the local optimal value of c is 5 as well.

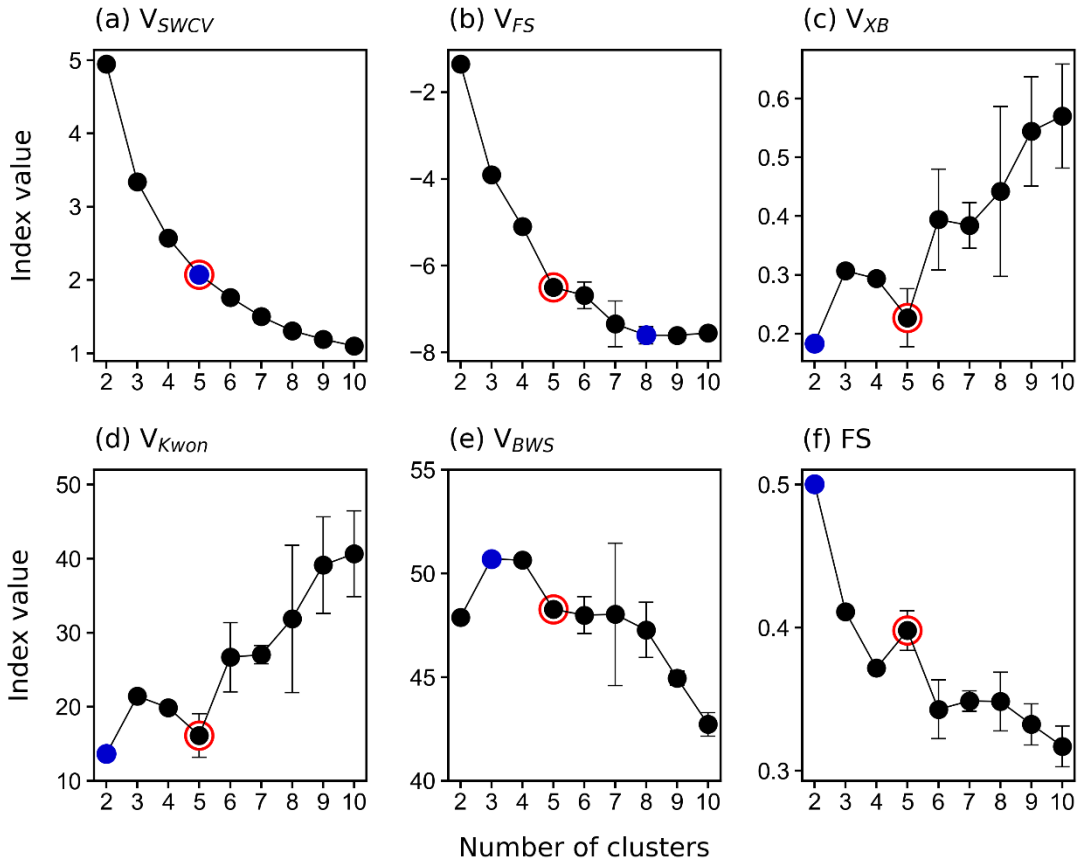


Figure 1. Values of selected clustering validity indices V_{SWCV} (a), V_{FS} (b), V_{XB} (c), V_{Kwon} (d), V_{BWS} (e), and FS (f) as a function of the number of clusters from 2 to 10. The averages of results from 50 repetitions are shown in the plot, and the error bars show the standard deviations. Blue points denote the optimal values of c according to each CVI, and the solution selected for further analysis is marked by red circles.

In addition, the Bouguessa-Wang-Sun index (V_{BWS}) and the Fuzzy Silhouette values (FS) were calculated for each FCM run. These two indices use slightly different definitions of compactness and separation to measure the quality of clustering. The V_{BWS} uses the fuzzy covariance matrix as a measure of compactness, and thus V_{BWS} takes cluster shape, density, and orientation into account and has been proven to work well for largely overlapping clusters (Bouguessa et al., 2006; Bouguessa and Wang, 2004). In general, the larger V_{BWS} is, the better a fuzzy partition will be, and hence the optimal number of clusters for our data is 3 (and 4) based on V_{BWS} (Fig. 1e). Meanwhile, as depicted in Fig. 1e, V_{BWS} shows that there is a local optimum at $c = 7$, though it has a higher uncertainty at this point. FS is an extension of the concept of Crisp Silhouette (CS) that was originally developed to assess non-

fuzzy clustering (Rousseeuw, 1987). It is more appealing than *CS* for fuzzy clustering since it
525 makes explicit use of the fuzzy partition matrix. In *FS*, objects in the near vicinity of cluster
centers are given more importance than those located in the boundary region (overlap).
Consequently, it performs better than *CS* for highly overlapping data (Campello and
Hruschka, 2006). In principle, a larger overall *FS* suggests a better partition. Therefore, the
530 best number of clusters determined by *FS* is 2 (Fig. 1f). Nevertheless, when $c = 2$, the sum of
the within-cluster variance for this solution is still quite high (Fig. 1a), which is not expected
for a good partition. It seems more sensible to set the number of clusters to 5, as this is where
FS reaches its local maximum and V_{SWCV} is significantly reduced and has the maximum
curvature. It is worth noting that the silhouette score can not only be used to assess the overall
quality of partition, but also to evaluate the quality of individual clusters and objects. The
535 silhouette score of an object ranges from -1 to +1, and a value close to +1 indicates that the
object is correctly assigned. On the contrary, a silhouette value of -1 implies that the object is
misclustered and should be assigned to a neighboring cluster. A silhouette value approaching
0 suggests that the object is in the overlapping region of clusters, and thus the algorithm is
unable to assign it to one cluster (Campello and Hruschka, 2006; Rawashdeh and Ralescu,
540 2012; Subbalakshmi et al., 2015).

In summary, different CVIs sometimes suggest a different optimal cluster number.
However, by making use of information from multiple CVIs, the appropriate number of
clusters in this study is determined to be 5. It should be noted that the main topic of this study
is to offer a proof of concept for the application of FCM in deconvolution of mass
545 spectrometric data. Therefore, the depth of the discussion about the determination of the
correct cluster number in this section must suffice for our purpose. The solution of $c=5$ is
selected here as one example for the chemical characterization and kinetic parameterization
in the following sections. In addition, It is worth mentioning that the multiple CVIs method
presented in this section provides a way to automatically determine the optimal number of
550 clusters for FCM.

3.1.2 Distance metric

Figure 2 shows four selected CVIs as a function of c with different distance metrics. As
mentioned before, smaller V_{FS} and V_{Kwon} indicate better partitioning, whereas for V_{BWS} and
FS, the opposite applies. In terms of V_{FS} , it indicates that the cosine distance is more suitable
555 for FCM in our case, although the impacts of different distance metrics on the clustering
outcomes are minimal (Fig. 2a). The V_{BWS} values also suggest that the cosine distance is

more appropriate for FCM regarding the data used in this study. As for V_{Kwon} and FS , there are no significant differences in the quality of partitioning when the number of clusters is small (e.g., $c = 2, 3, 4$) despite different distance metrics, as shown in Fig. 2b and Fig. 2d. However, the discrepancies become more pronounced with increasing c . In general, the Euclidean distance is more appealing for our data in terms of V_{Kwon} and FS . To conclude, among all the examined distance metrics, the Euclidean and cosine distance provided a better performance in fuzzy clustering regarding the data used in this study, and the Euclidean distance was employed as the (dis)similarity metric in FCM for further analysis in this study. Additionally, the Euclidean distance was used in the calculation of various CVIs.

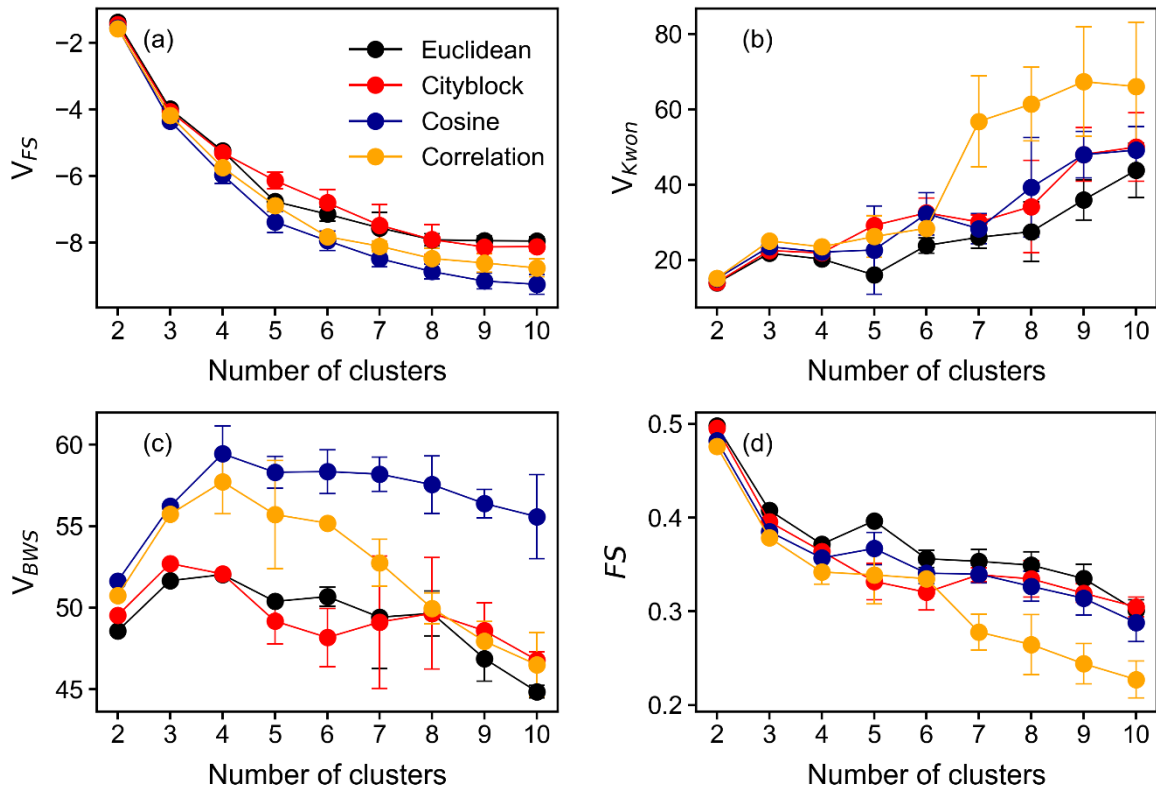
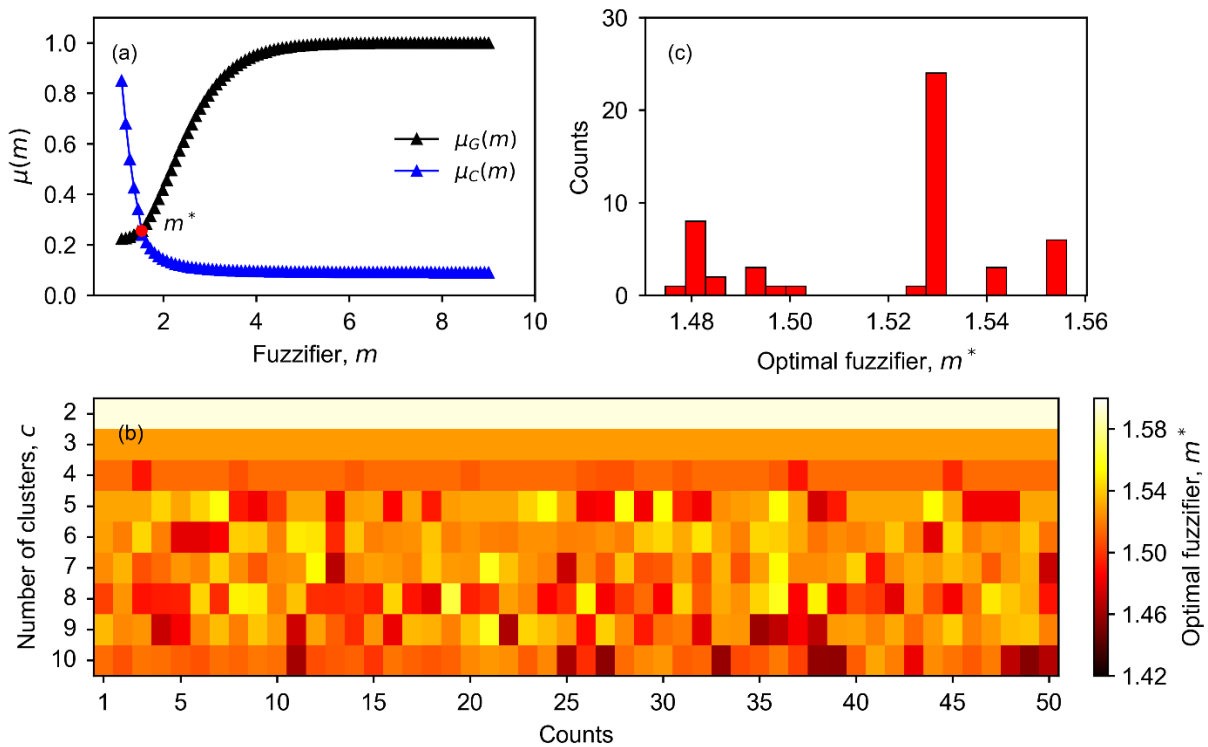


Figure 2. Values of selected clustering validity indices V_{FS} (a), V_{Kwon} (b), V_{BWS} (c), and FS (d) as a function of the number of clusters. Points in different colors are results obtained with different distance or similarity metrics. The averages of results from 50 repetitions are shown in the plot, and the error bars denote the standard deviations. Euclidean distance was used in the calculation of CVIs.

3.1.3 Fuzzifier value

Based on the fuzzy decision-making method introduced in Sect. 2.3.3, we searched m^* in the
575 range of [1.1, 9] with an increment of 0.1. The intersection of the fuzzy objective function, μ_G ,
and the fuzzy constraint, μ_C , as shown in Fig. 3a, indicates the optimal value of the fuzzifier
for each run. To investigate whether m^* depends on c and/ U^0 , the number of clusters was set
to vary from 2 to 10. For each c in this range, FCM was performed 50 times with a randomly
created initial fuzzy partition matrix.

580 As shown in Fig. 3b, we do observe a relationship between m^* and c/U^0 . For smaller
cluster numbers, e.g., $c = 2$ or 3, the determined optimal values of m are slightly larger than
those obtained with larger c ($c \geq 4$). In addition, the results obtained with a smaller c are
more robust. Different repetitions always return identical m^* , which suggests that the initial
fuzzy partition matrix does not affect m^* when the number of clusters is smaller than 4.
585 However, when c increases to 4 or even larger, there is a variation in m^* among different
repetitions, indicating that U^0 starts to affect the determined value of m^* , even though the
variation of the value of m^* is small (between 1.42 and 1.52). One plausible explanation for
the dependency of m^* on c/U^0 is shown as follows. When c is small, there are more overlaps
between clusters and thus m^* can be relatively large. When c becomes larger, the assignment
590 becomes “stricter” and the overlaps between clusters are reduced. Therefore, m^* gets smaller,
and the clustering outcomes become more specific, which are likely to be more sensitive to
local minima. Since the local minima largely depends on U^0 , consequently, the results
become more sensitive to U^0 .



595

Figure 3. Determining the optimal value of the fuzzifier (m^*) in FCM. In panel (a), the intersection (red point) of the fuzzy objective function (μ_G) and constraint (μ_C) is determined as m^* . Panel (b) depicts the relationship between m^* , the number of clusters (c), and the initial fuzzy partition matrix (U^0). Panel (c) shows the frequency distribution of m^* for 50 repetitions with $c = 5$ (determined as the optimal number of clusters in this study).

600

Figure 3c displays the distribution of m^* obtained from 50 repetitions with $c = 5$. The histograms of the optimal value of m with other numbers of clusters are provided in the supplement (Fig. S3). For $c = 5$, the results suggest that the optimal value of m is 1.53 in most cases. Therefore, a value of $m = 1.53$ is used for the FCM in this study.

605

Overall, the number of clusters and the initial membership degree matrix do affect the optimal value of the fuzzifier that was determined based on the fuzzy decision-making method in this study, but the influence is not very strong. The values of m^* determined for our data set vary around 1.5 despite different c and U^0 , indicating that the FCM results in this study are relatively crisp.

610 3.2 FCM clustering results

3.2.1 FCM of chamber data

Using the appropriate clustering parameters determined in Sect. 2.3, we performed FCM to chamber data with the number of clusters varying from 2 to 10. For each c , the algorithm was run 50 times. According to the results of these 50 repetitions, two- and three-cluster solutions
615 seem very robust. The repetitions always give identical outcomes despite different initial partition matrices. This is also true for the five-cluster case. However, the influence of the initial position of the cluster centers on the partition increases when the number of clusters is further increased, but in all cases, more than half of the repetitions return the same results; thus, we select the most frequent outcomes as the final solutions for each case. Here we will
620 not describe all solutions in detail, but instead, try to formulate a synthesis of the results and present the common features shared by solutions with different numbers of clusters.

Figure 4 shows the FCM results with 2-5 clusters for the chamber data obtained during the isoprene-NO₃ experiment. Additional solutions with 6-10 clusters are shown in the Supplement (Fig. S4). Two distinct clusters emerge from the data in the two-cluster solution.
625 According to their relative formation rates, cluster 1 is regarded as first-generation cluster since species belonging to this cluster show a pronounced signal increase after addition of the reactants, while cluster 2 behaves more like second or later-generation products with its overall formation rate being much smaller than that of cluster 1. In addition to the time patterns, the mass profiles of cluster 1 and cluster 2 are clearly different (Fig. 4b).

630 When the cluster number is increased to 3, both, the time pattern and the mass profile of cluster 1, almost remain unchanged compared to those in the two-cluster case. It seems that mainly the former cluster 2 is separated into two new clusters (cluster 2 and 3) with different formation rates for each. Cluster 2 is regarded as a representative of the second-generation processes, and cluster 3 represents third- or later-generation products since it exhibits a
635 smaller formation rate compared to cluster 2. However, there are less high-affiliation members (with a membership degree over 0.5) in cluster 1 in the three-cluster solution, indicating that at least some of the former contributors of this cluster have been moved, most likely to the new cluster 2. The mass profiles of cluster 2 and cluster 3 display quite distinct features, as shown in Fig. 4b, but the mass profiles of cluster 2 in both the two- and the three-
640 cluster solution match to a large extent, even though their time patterns are somewhat different.

As shown in Fig. 4b, part of the species from cluster 1 in the three-cluster solution is separated out to a new cluster (cluster 2 in four-cluster solution) when increasing the number of clusters from 3 to 4. The newly formed cluster shares the same fingerprint molecules, i.e.,
645 $C_5H_9NO_5$ and $C_5H_9NO_6$ (corresponding to species no. 34 and no. 38 in Fig 4b), in the mass profile with cluster 1 in three-cluster case. This migrates the former cluster 2 into cluster 3, and cluster 3 into cluster 4, with some slight alterations in their time patterns and mass profiles. The time series of the new cluster 2 resembles that of cluster 1, but with smaller formation rates. In general, the member traces of different clusters seem to converge towards
650 the time traces of the cluster centers, indicating that the system approaches the correct number of clusters.

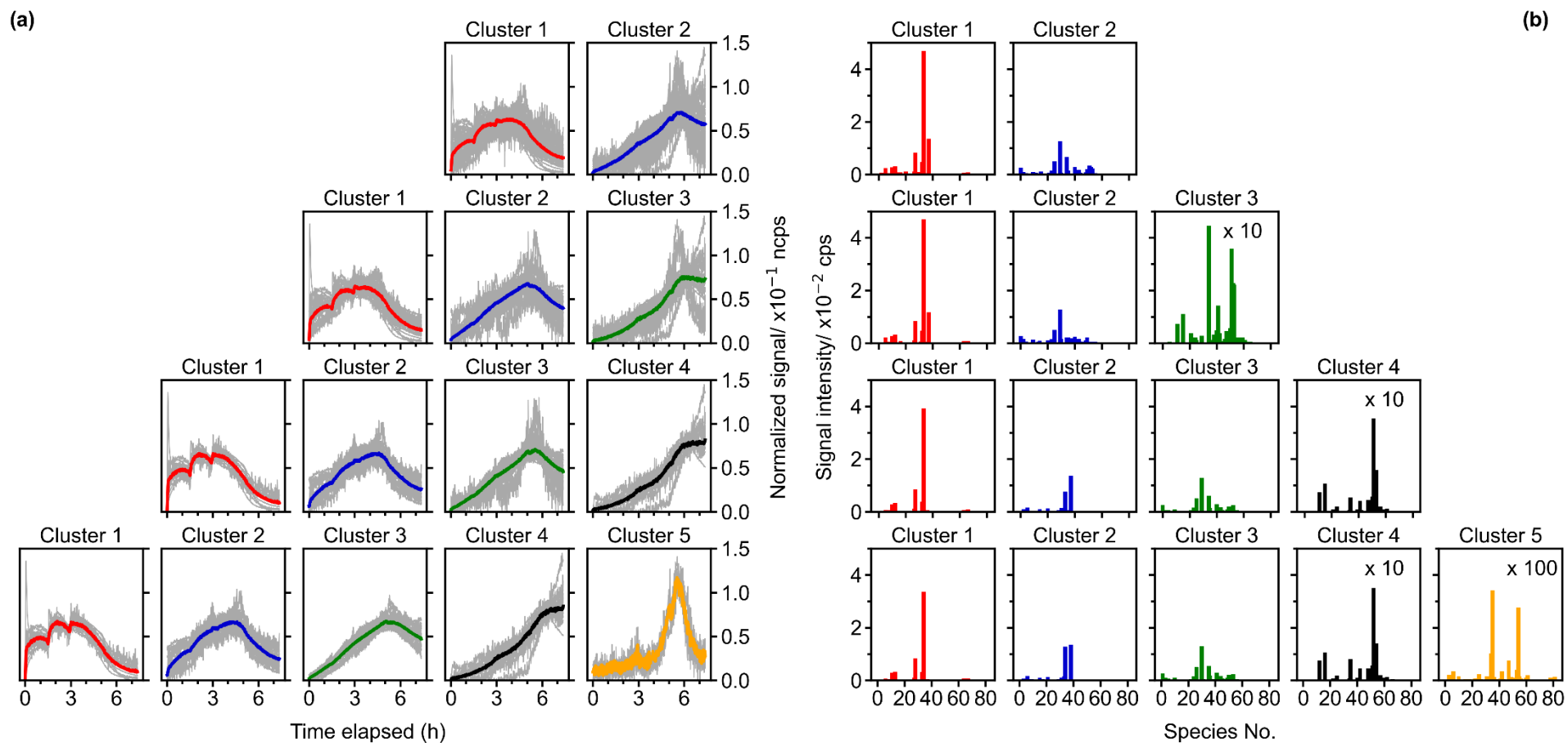
When increasing the number of clusters from 4 to 5, a new, distinct cluster (cluster 5) emerges, which has very small production in the early reaction stage, and its time trace shows that members in this cluster were destroyed significantly when there was abundant NO_3 in the
655 system (Step IV in Fig. S1). This specific character in time seems to evolve already in cluster 4 in the four-cluster solution. The mass profiles of the first four clusters of the five-cluster solution are very similar to those of the four-cluster case, but the mass profile of cluster 5 shows distinct differences from that of the others. It is important to mention that these five clusters now also effectively capture the loss rates over a time scale larger than 13h, and that
660 most members in these clusters are well represented by their respective cluster centers.

When the number of clusters is further increased, more detailed and complicated clustering outcomes emerge, which is impelled by different formation and/or destruction pathways of species (Fig. S4). However, the differences between the new and existing clusters become smaller. Since the major objective of this study is to demonstrate the
665 applicability of FCM in analyzing mass spectrometric data, we will not discuss the detailed interpretation of these solutions here.

To better understand the chemical composition of clusters, the bulk chemical properties like hydrogen-to-carbon ratio (H:C), oxygen-to-carbon ratio (O:C), and average carbon oxidation state (\overline{OS}_C) of different clusters were calculated and compared. The \overline{OS}_C of each
670 cluster was calculated following the method proposed by Kroll et al (2011), in which all the N atoms of N-containing compounds were assumed to be present in nitrate groups (and thus $OS_N = +5$), as described in our previous study (Wu et al., 2021). Figure 5 shows the distribution of clusters in the \overline{OS}_C vs. n_C space for solutions with 2 to 5 clusters. Additional results for solutions with 6 to 10 clusters can be found in the supplement (Fig. S5). The

675 contribution of an individual species to a cluster is weighted by its nominal mass and signal
intensity in the cluster profile. Regardless of the number of clusters, different solutions cover
similar chemical composition ranges in terms of average \overline{OS}_C and n_C . However, there are
discrepancies in detail. For example, the \overline{OS}_C of cluster 5 in the five-cluster solution slightly
680 deviates from the trend that the other four clusters follow. A similar behavior is observed for
cluster 1 in the six-cluster solution. This indicates that increasing the number of clusters
could help to find new groups of species with distinct chemical compositions. However,
further increasing the number of clusters to 7 or more clusters does not yield new clusters
with significantly different chemical composition, implying that $c = 5$ or 6 is the appropriate
685 number of clusters in terms of separation by chemical composition. It is also shown in Fig. 5
that different clusters are well separated in the \overline{OS}_C vs. n_C space despite some overlaps,
indicating that they have distinct chemical compositions. For instance, the two early-
generation clusters, cluster 1 and cluster 2 in the four-cluster solution, are differentiated in
chemical properties from each other.

In general, the early-generation clusters with lower oxidation degree fall in the corner of
690 the plot with smaller \overline{OS}_C but larger n_C , while the later-generation clusters with higher
oxidation degree move towards the corner with larger \overline{OS}_C but smaller n_C . This indicates that
the later-generation products detected in the gas phase in this study were formed through
further oxidation of early-generation species and they underwent more fragmentation during
oxidation. Of course, it is very likely that there are later-generation products with larger n_C .
695 However, as they become highly functionalized through multiple oxidation steps, they would
have a very or extremely low volatility and thus only/ mostly exist in the particle phase,
undetectable in the gas phase.



700

Figure 4. Results of fuzzy c -means clustering for chamber data with cluster numbers between 2 and 5: Time series (a) and mass profiles (b) of clusters for each solution (in row). The time series of cluster centers are shown as thick, colored solid lines, and the time series of species with the membership degree larger than 0.5 to the cluster are illustrated as thin, gray lines. The species number in panel (b) corresponds to species listed in Fig. S7 (in order of molecular mass).

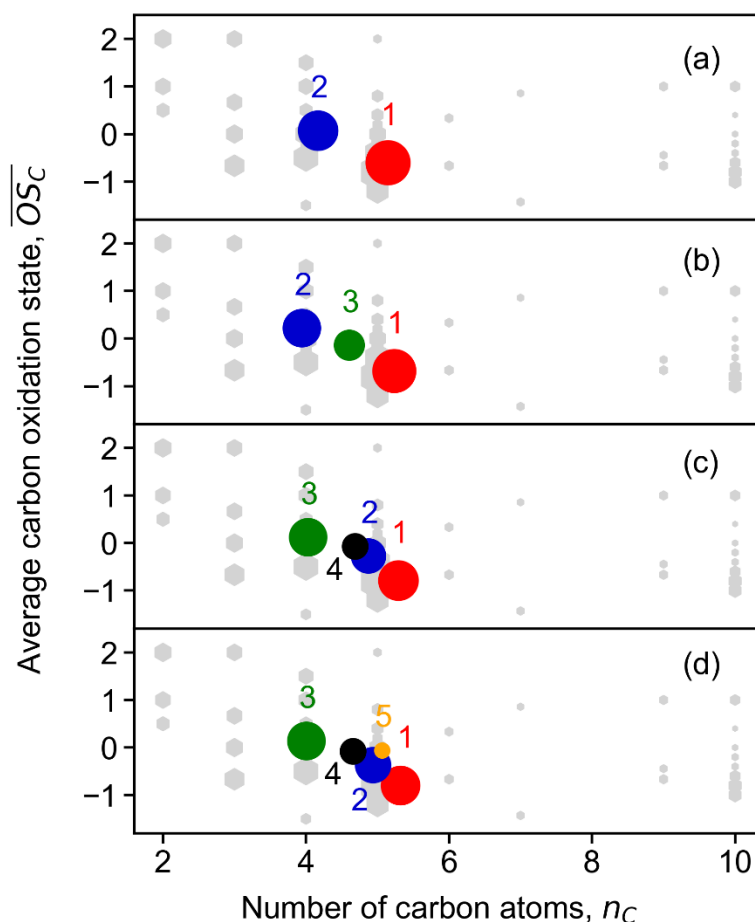
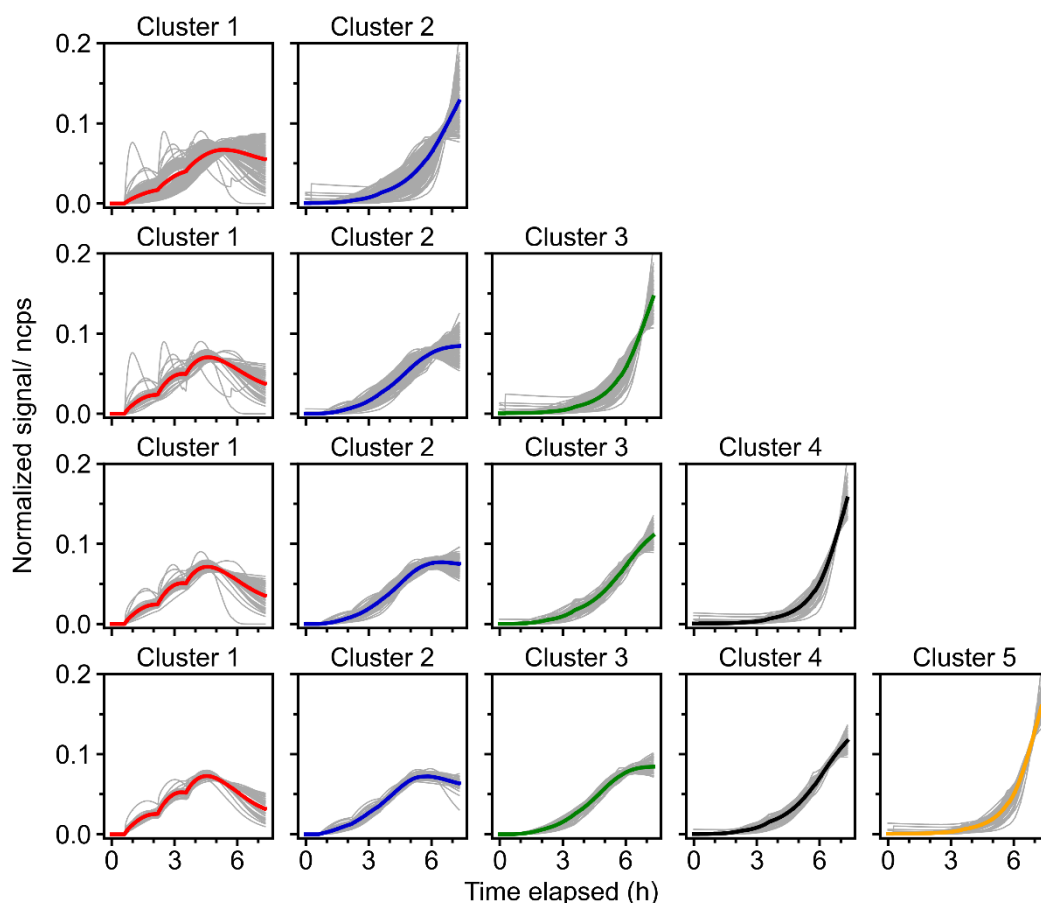


Figure 5. Average carbon oxidation state (\overline{OS}_C) of the obtained FCM clusters from chamber data as a function of number of carbon atoms (n_C). Panel (a) to panel (d) show results for solutions with 2 to 5 clusters, respectively. Cluster centers are depicted by circles in different colors. The color scheme follows that in Fig. 4. The marker area of clusters is proportional to the sum of average signal intensity of all species in the cluster weighted by their membership degrees. Closed-shell products detected by Br⁻ CIMS are shown as grey hexagons, and the marker area is proportional to the average intensity of species over the whole experiment.

3.2.2 FCM of model data

As mentioned earlier, we also applied FCM to data obtained from a box model, with the default gas-phase reaction schemes for isoprene-NO₃ taken from the MCM v3.3.1 (Jenkin et al., 2015). For consistency, only closed-shell products from isoprene oxidation in MCM were taken for the clustering. Since the reaction scheme of isoprene with NO₃ in the MCM mechanism is semi-explicit, the clustering results of modelled data provides a way to evaluate the applicability of fuzzy clustering in analyzing time series data. In turn, by comparing the cluster centers derived from model data with those derived from mass spectrometric data, one can check if the model can well reproduce the measurements, and thus investigate the representativeness of oxidation mechanism coupled in the model.

725 Figure 6 shows the results of FCM applied to model data, again with the number of
clusters varying from 2 to 5. It is clearly shown that different species are sorted according to
their patterns of time behaviors, and that different clusters represent multi-generation
products. Taking the 2-cluster solution as an example, the signals of most species in cluster 1
increase evidently as soon as the reaction is initiated, while those in cluster 2 grow
730 considerably slow, indicating that cluster 1 is a surrogate of early-generation products,
whereas cluster 2 corresponds to later-generation products. This is very similar to what we
observe from the real measurements, even though the time behavior derived from those two
cases are not the same. However, the fast-forming pathways play a more important role in the
measured data than in the model data. In addition, more later-generation clusters are selected
out from the model data with increasing number of clusters, whilst the changes in early-
735 generation clusters are indistinct. However, in terms of clusters 3-5 in the five-cluster
solution, it is evident that certain chemical loss processes are missing in the MCM
mechanism, which are observed from the chamber data. For instance, autoxidation and
related processes for the isoprene + NO₃ system are underrepresented in the MCM, as well as
the formation of accretion products.



740

Figure 6. Results of FCM for model data with the number of clusters varying from 2 to 5. Each row represents one solution, with the time series of cluster centers shown in thick, colored solid lines, and species with the membership degree larger than 0.5 to the cluster illustrated as thin, gray solid lines.

745

As for the chemical properties, different clusters are discrete in the \overline{OS}_C vs. n_C space (Fig. S6), and thus it can be inferred that product species would also be grouped in a reasonable way when applying FCM to experimental data. Moreover, clusters in different solutions cover a similar chemical composition range of \overline{OS}_C and n_C despite increasing number of clusters (except for the two-cluster solution), well consistent with what we observed for the chamber data. However, the increase in the \overline{OS}_C of clusters for model data is less pronounced during the oxidation processes, probably due to the absence of autooxidation steps in the MCM. Moreover, the MCM lacks accretion products (mostly assigned to early-generation clusters with more carbon atoms in bulk), but tends to have more small species (with low n_C), which is not observed in the mass spectra data. This can be due to the detection limits of the Br-CIMS for smaller compounds. Regarding the two-cluster solution, the chemical range of clusters is much narrower, and they are overlapping in the chemical space to some extent, suggesting that the number of clusters is not enough.

755

According to the outcomes from the application of FCM to both measured and model data, we conclude that FCM can give interpretable and chemically meaningful results when it is applied to mass spectrometric data in time series analysis.

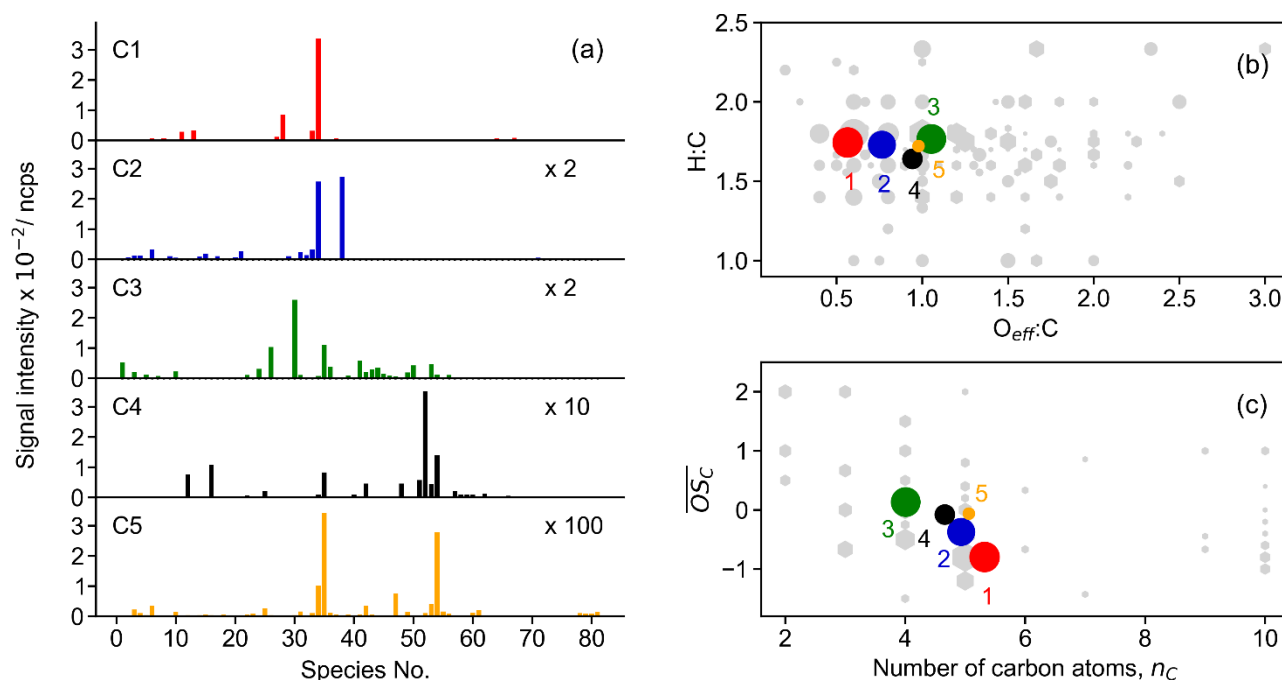
3.3 Insights from clustering results

3.3.1 Chemical properties of different clusters

In this section, we utilize the five-cluster solution, identified as the optimal cluster number for our dataset (Sect. 2.3), to illustrate how to extract chemical and kinetic information from the mass spectrometric data based on the FCM analysis. This does not necessarily mean that the five-cluster solution is superior over others. However, as demonstrated in previous sections, the FCM results exhibit consistent features regardless of the number of clusters predefined. Therefore, findings derived from the five-cluster solution could potentially apply to other cases.

It is clearly shown in Fig. 7a that different clusters have significantly different compositions. For example, cluster 1, which represents the early-generation products, is dominated by a single species (with the chemical formula $C_5H_9NO_5$), and its intensity is much higher than those of the other four clusters. Another characteristic of cluster 1 is that more than 80% of detected 2N-dimers (except one species with the formula $C_{10}H_{16}N_2O_{11}$) are assigned to this cluster (Fig. S7). These compounds are obviously first-generation products probably formed through $RO_2 + RO_2$ reactions (Wu et al., 2021). Therefore, it is reasonable to sort them into cluster 1, which is representative for the early-generation products. Cluster 2 also behaves like early-generation products, but differs from cluster 1 in terms of reactivity, i.e., formation and destruction rates. The differences of cluster 1 and cluster 2 in chemical composition are even more perceptible. As shown in Fig. 7a, besides $C_5H_9NO_5$, there is another 1N-monomer ($C_5H_9NO_6$) present in cluster 2 with a relatively high intensity. In addition, most of the detected small molecules ($C_{\leq 3}$) are assigned to this cluster (Fig. S7). Note that the formation rate of cluster 2 (from FCM analysis of the chamber data) resembles that of cluster 1 (in the five-cluster solution) from FCM analysis of the model data. In addition, the fractions of some 3N-dimers (e.g., $C_{10}H_{17}N_3O_{12-14}$) in cluster 2 are relatively high (Fig. S7). 3N-dimers are expected to be second or even later-generation products that are produced from the cross reaction of a first-generation nitrooxy peroxy radical and a secondary dinitrooxy peroxy radical, or from further oxidation of the corresponding 2N-dimers (Wu et al., 2021). This indicates that cluster 2 is very likely a mixture of the first- and

790 second-generation products, which have not been resolved by FCM in the five-cluster
 solution. Increasing the number of clusters might help to separate the typical behavior of a
 minority of components. When the cluster number is increased to 6, it is indeed mainly the
 former cluster 2 in the five-cluster solution which is further split into new clusters (cluster 2
 and cluster 3), in which the first-generation behavior of the new cluster 2 is more pronounced.
 795 From this point of view, the six-cluster solution seems better than the five one.



800 **Figure 7.** Chemical properties of clusters from the five-cluster solution. The subplots show
 mass profile of each cluster (a), van Krevelen plot (b), and average carbon oxidation state of
 clusters (c), respectively. Different clusters are distinguished by color, and the color scheme
 follows that in Fig. 4. The marker area of clusters is proportional to the sum of average signal
 intensity of all species in the cluster weighted by their membership degrees. The species
 number in panel (a) corresponds to species listed in Fig. S7 (in order of molecular mass).
 805 Grey hexagons in panel (b) and panel (c) denote species identified by Br⁻ CIMS, and the
 marker area is proportional to the average intensity of species over the whole experiment.

Regarding later-generation clusters, namely cluster 3, cluster 4 and cluster 5, the second-
 or later-generation products, such as C4 species, 2N- and 3N-monomers, are predominant in
 their composition. Nevertheless, the mass profiles of cluster 3, cluster 4, and cluster 5 are
 quite distinct. For example, cluster 3 is dominated mainly by a C4 species (C₄H₇NO₅), while
 810 the major fingerprint of cluster 4 is constituted by two 2N-monomers (C₅H₈N₂O₈ and
 C₅H₈N₂O₉), a C4 species (C₄H₇NO₆), and a C2 species (C₂H₃NO₅). In addition, 3N-
 monomers are almost completely present in cluster 4 (Fig. S7). Cluster 5 has a much lower

intensity compared to other clusters, and a distinctive characteristic of this cluster is a high contribution of two 3N-dimers ($C_{10}H_{17}N_3O_{15}$ and $C_{10}H_{17}N_3O_{16}$) (Fig. S7).

815 Figure 7b and 7c show the chemical properties of each cluster center in terms of the bulk elemental molar ratios (in the Van Krevelen space), and the average carbon oxidation state. The Van Krevelen plot visualizes the chemical composition of organics by hydrogen-to-carbon (H:C) vs. oxygen-to-carbon (O:C) ratio, and it is widely used to trace the origin and evolution of organic compounds (Chhabra et al., 2011). When calculating the O:C ratios of
820 N-containing compounds, the concept of effective oxygen number (n_{O_eff} , $n_{O_eff} = n_O - 2 * n_N$) was employed, where in the case of a nitrate group, only one of the O atoms bonded to C atom was considered in the calculation (Xu et al., 2021). The cluster centers cover a narrow range of chemical space of the original dataset (grey circles in Fig. 7b), but are located where most of the compounds fall in. They lie almost along a line of H:C = 1.75 in
825 the Van Krevelen plot, indicating that they have gained on average one H atom compared to isoprene. A trajectory with slope zero is expected in van Krevelen plots when only alcohol or hydroperoxide functionalities are introduced in the molecule (Chhabra et al., 2011). This is a characteristic of autoxidation steps (-O₂H) or H-shifts in alkoxy radicals (-OH, and thereafter -O₂H). Therefore, the distribution of the clusters in the Van Krevelen space implies that
830 autoxidation steps or intramolecular H-shifts were involved in the reactions of isoprene with NO₃ studied in this work.

In terms of average oxidation state and carbon atom numbers, the early-generation products which undergo less oxidation steps usually have much lower oxidation degree but more carbon atoms per molecule. With the reaction proceeding, the early-stage products will
835 be further oxidized and fragmented, leading to the formation of later-generation products with a higher oxidation state but less carbon atoms per molecule. Consequently, the trajectory of chemical processes generally starts with the precursor in the right lower corner and moves towards to the left upper area (products) in the \overline{OS}_C vs. n_C space through oxidation and fragmentation. In this study, the early-generation clusters have a lower oxidation state but
840 more carbon atoms while the later-generation clusters are the other way around, well following the oxidation trajectory in chemical space.

When considering the characteristics of members in each cluster, we focus solely on high-affiliation species (with a membership degree over 0.5) to simplify the discussion. Figure 8 shows the chemical properties of the high-affiliation species described by their
845 elemental molar ratios and average carbon oxidation state. In general, most of the high-

affiliation species of the two early-generation clusters (cluster 1 and 2) center in a relatively low $O_{\text{eff}}:C$ area of the van Krevelen plot, while those from the three later-generation clusters (cluster 3, 4, and 5) spread to the higher $O_{\text{eff}}:C$ area. This confirms that species belonging to later-generation clusters are generally more oxidized than those from early-generation clusters, as expected. With respect to the average oxidation state, species of cluster 1 in general have lower \overline{OS}_C than others, and they are mainly monomers ($n_c = 5$) and dimers ($n_c = 10$). The \overline{OS}_C of species from cluster 2 is slightly higher than that from those of cluster 1, and there are more fragments in this cluster, including both monomers with $n_c < 5$, and dimer species with $5 < n_c < 10$. The high-affiliation species of later-generation clusters generally have higher oxidation degree than that from early-generation clusters, but most of them are molecules with less than 6 carbon atoms.

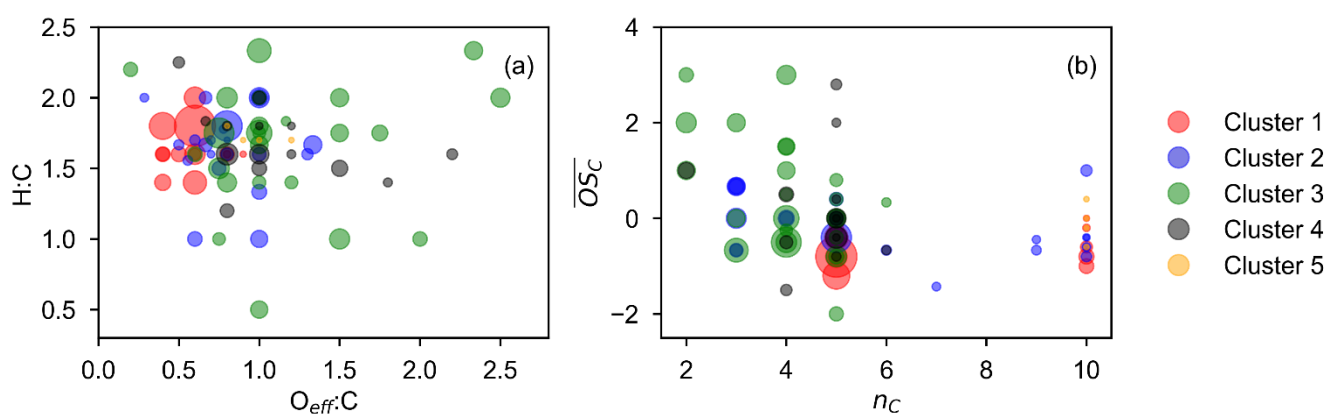


Figure 8. Chemical properties of high-affiliation species from each cluster (with a membership degree larger than 0.5) described by van Krevelen (a) and average carbon oxidation state (\overline{OS}_C) vs. carbon number (n_C) (b) plot. The marker area is proportional to the average signal intensity of species over the whole experiment.

Based on abovementioned results, we conclude that FCM is a feasible dimension-reduction technique for dealing with complex mass spectrometric data from an oxidation system of interest. The derived clusters show a chemical realistic time behavior and cover the major range of chemical properties of the original dataset. This suggests that FCM could be useful in simplification and analyzing mass spectra data and the chemical information underlying in the clusters can be helpful to understand the system of interest.

3.3.2 Kinetic properties of different clusters

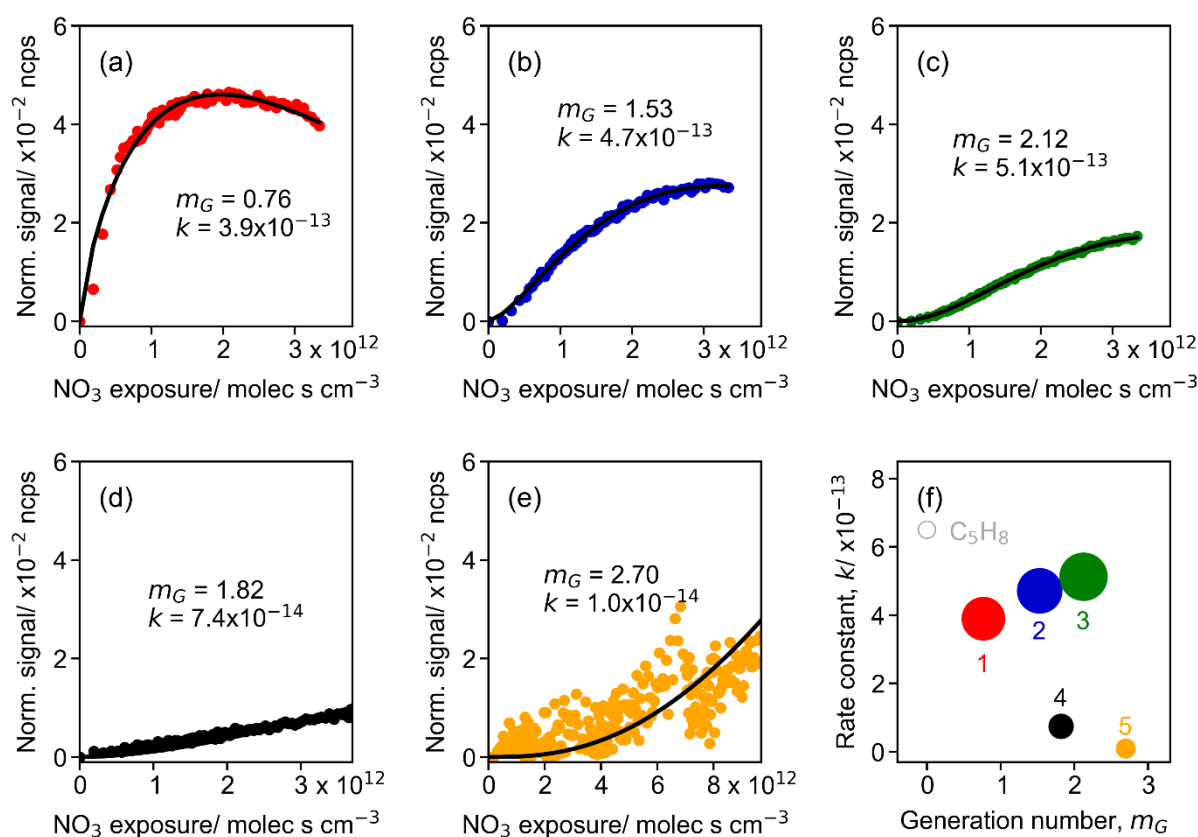
The FCM results shows that different clusters have different time behaviors, indicating that they were formed by different (or a series of) reaction steps. By fitting the GKP function (Eq. 12) to the measurements, we can extract underlying kinetic information (effective rate constant k and generation number m_G) from time series data. Generally, a larger value of k

implies a faster formation rate of a product class for a given oxidant exposure and vice versa. It should be noted that the k obtained here is not a stepwise rate constant, and it has no direct relationship to the stepwise rate constants of the reaction sequence. However, this value offers a way to quantitatively measure the overall rate constant of all reactions along the pathway (Koss et al., 2020). Since the FCM cluster centers represent chemically realistic time patterns and retain the major kinetic properties of the original dataset, they can be used as surrogates for various products formed in the isoprene-NO₃ system, and the GKP function can be fitted to the time series of cluster centers. This largely reduces the complexity of data analysis and provides a way to get kinetic information directly from measurements.

Figure 9 shows the result of the fit of GKP to the FCM clusters derived from the chamber measurements for the five-cluster solution. All except cluster 5 fit with a coefficient of determination (r^2) of 0.96 or higher, indicating that the GKP model can well reproduce the kinetic behavior of the products formed from the isoprene-NO₃ oxidation system in this study. Cluster 5 is not well reproduced (with a r^2 of 0.41), probably due to its extremely low and noisy signal as a surrogate of later-generation products. The fitted values of m_G for early-generation clusters are expected to be 1 in theory. As depicted in Fig. 9a, the generation number of cluster 1 is close to 1, and that of cluster 2 is between 1 and 2, coinciding with the expectation. As for the three later-generation clusters, their m_G values are approximately 2 (cluster 3 and 4) or 3 (cluster 5), indicating that they undergo two or more NO₃ oxidation steps.

There are several possible reasons for non-integer values of m_G , including uncertainties from signal noise, especially for low signal-to-noise data, and possible influences from physical processes like vapor-wall interaction, which can lower the signal of species and thus lead to a higher fitted m_G . (Koss et al., 2020). In addition, the value of m_G can be distorted to some extent if compounds are produced from isoprene oxidation by oxidants other than NO₃, e.g., OH and O₃ in this case. While NO₃ makes up the major fraction of consumption of isoprene, its reactions with O₃ and OH still contribute for 10-15% of isoprene loss (Vereecken et al., 2021, Carlson et al., 2022). Consequently, it is very likely that some species detected by CIMS were oxidized by multiple oxidants. Such an effect will lower m_G , as unaccounted sources increase the concentrations of species besides the NO₃ exposure, and the linear, first-order kinetic assumption of the GKP model is no longer applicable. For example, the isoprene hydroperoxy aldehyde (C₅H₈O₃), one of the major products from photooxidation, is also observed from NO₃-initiated oxidation (Vereecken et al., 2021;

Wennberg et al., 2018; Wu et al., 2021). Furthermore, the deviation of m_G from integer values can occur if isomers that were formed by a different number of oxidation steps exist.



910 **Figure 9.** Parameterized effective rate constant (k , $\text{cm}^3 \text{ molecule}^{-1} \text{ s}^{-1}$) and generation number
 (915 m_G) for FCM clusters (five-cluster case) derived from CIMS measurements of isoprene- NO_3
 system. Panels (a) to (e) show GKP fitting results for different clusters, with cluster 1 in red,
 cluster 2 in dark blue, cluster 3 in green, cluster 4 in dark, and cluster 5 in orange,
 respectively. Colored dots in each panel are time series of clusters, and black lines are GKP
 915 fits. Panel (f) shows the distribution of kinetic parameters. Marker area is proportional to the
 sum of average intensity of all species in the clusters weighted by their membership degrees.

Since the generation number corresponds to the reaction steps with NO_3 to form the product, the later-generation species, which undergo more oxidation steps, should have larger m_G values and higher nitrogen-to-carbon ratios (N:C) when considering NO_3 is the only
 920 oxidant. Figure 10 shows the relationship between generation number and chemical properties of clusters. In general, clusters with higher m_G have larger N:C ratios, as expected, confirming that NO_3 is the predominate oxidant for isoprene oxidation in our system. Nonetheless, we find that species with larger N:C ratios are not necessarily later-generation products. As shown in Fig. 9a, cluster 4 has a larger N:C ratio than cluster 3 and cluster 5, but
 925 it turns out with a smaller m_G . This indicates that some of the nitrogen atoms of compounds in cluster 4 were gained through non-oxidative steps. On the other hand, cluster 5 has a larger

m_G value than cluster 3 and cluster 4, but its N:C ratio is relatively small. This is probably because the species in cluster 5 were formed by isoprene oxidation by other oxidants than NO_3 , e.g., OH and O_3 . Another plausible explanation could be that the NO_3 oxidation reaction does not lead to an increase in nitrogen content in the product molecules, e.g., through H-abstraction instead of addition to C=C double bonds (Wu et al., 2021).

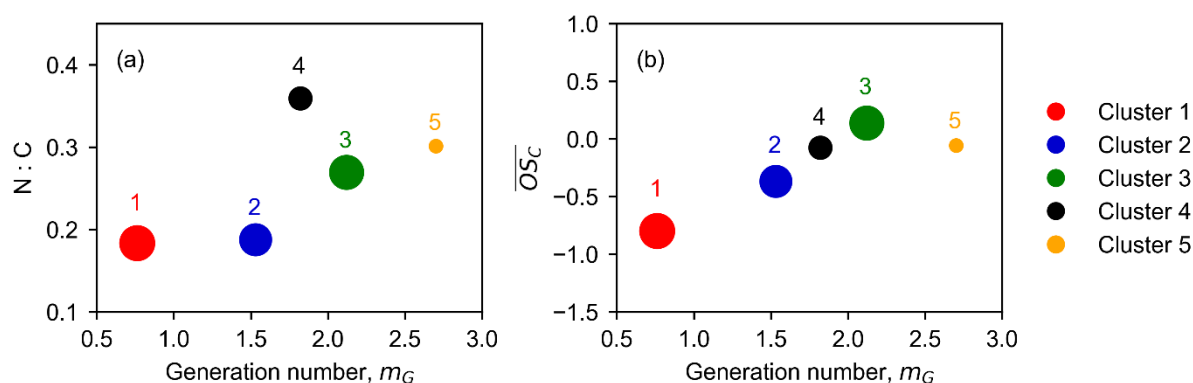


Figure 10. Relationship between generation number (m_G) and chemical properties of clusters: Nitrogen-to-carbon (N:C) ratio (a) and average carbon oxidation state (\overline{OS}_C) (b) as a function of m . The marker area is proportional to the sum of average intensity of all species in the clusters weighted by their membership degrees.

There is a strong linear correlation between the generation number and the average oxidation state of the clusters apart from cluster 5, as illustrated in Fig. 10b. The early-generation clusters have smaller m_G values than later-generation clusters, which corroborates that the generation number returned by the GKP model is reasonable. The linear regression result shows that the value of \overline{OS}_C increases by ~ 0.74 for each generation. For $m_G = 0$, the corresponding \overline{OS}_C is -1.45 , approximate to the average carbon oxidation state of isoprene ($\overline{OS}_C = -1.6$). For each addition of NO_3 functionality, the \overline{OS}_C of the corresponding product increases by 0.2, and the following O_2 addition (if possible) results in the \overline{OS}_C increasing by additional 0.8. Therefore, it involves at least one autooxidation step for each NO_3 addition considering an increase of about 0.8 in \overline{OS}_C per generation.

Cluster 5 has a m_G value approaching 3, suggesting that species belonging to this clusters roughly underwent three oxidation steps. However, its average oxidation rate is unexpectedly low, deviating from the linear line of m_G and \overline{OS}_C . One plausible explanation for this is that such species are probably formed through unimolecular fragmentation. For example, if the H-abstraction (of RO_2) occurs at a carbon with an $-\text{OOH}$ functionality attached, the reaction chain will be terminated by OH loss and lead to the formation of a

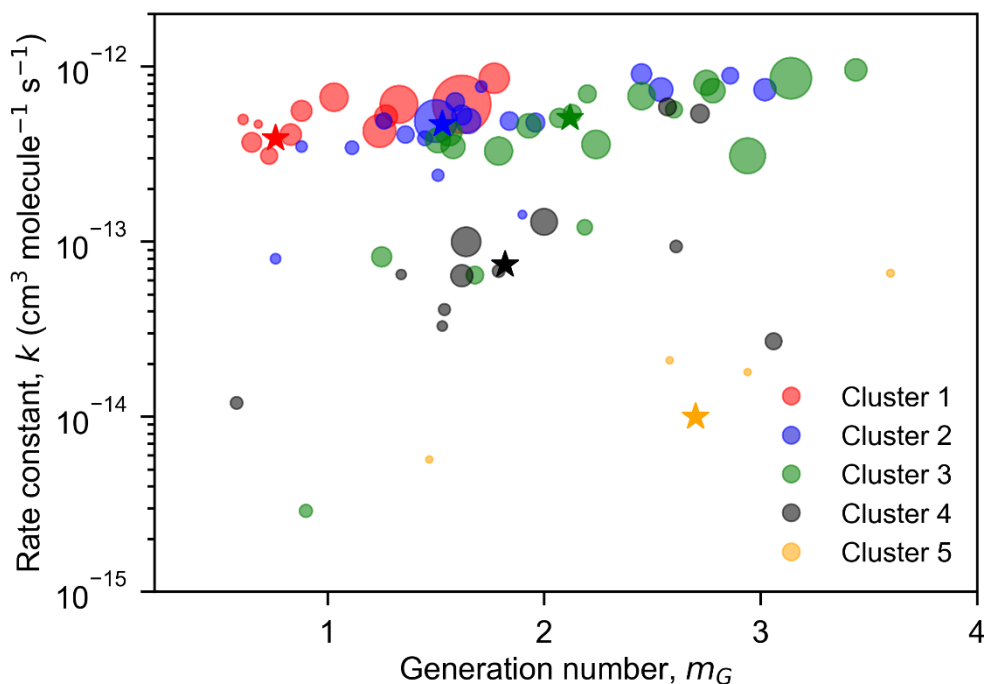
carbonyl compound (Bianchi et al., 2019), which results in products with a lower average
955 oxidation state.

In general, the effective rate constants of the clusters are limited by the reaction rate
constant of isoprene, and the early-generation clusters have larger k values than the later-
generation ones. As shown in Fig. 9f, the returned k values of the two early-generation
960 clusters 1 and 2 are very close to the reaction rate constant of isoprene with NO_3 (6.5×10^{-13}
 $\text{cm}^3 \text{ molecule}^{-1} \text{ s}^{-1}$ at 298K, IUPAC). The k values of the later-generation clusters, cluster 4
and 5, are about one order of magnitude smaller. Cluster 3, which represents second-
generation products with $m_G \approx 2$, has a similar effective rate constant as cluster 1 and cluster
2, indicating that the species belonging to this cluster form or react relatively fast. As shown
in Fig. 7c, cluster 3 has a high oxidation degree, but less carbon atoms on average, suggesting
965 that the species in cluster 3 are probably highly oxidized fragments. This is confirmed by its
mass profile (Fig. 7a).

The GKP method was also applied to individual species. Examples of fits for various
species are shown in Fig. S8. Figure 11 depicts the fitted k and m_G values of the high-
affiliation species from each cluster. For species from cluster 1, cluster 2, and cluster 3, most
970 of the returned k values fall in the same order of magnitude to the rate constant of isoprene
with NO_3 ($k = 6.5 \times 10^{-13} \text{ cm}^3 \text{ molecule}^{-1} \text{ s}^{-1}$ at 298K). For those from the two later-generation
clusters, cluster 4 and 5, the returned k values are about one, and two order(s) of magnitude
smaller, respectively. Most returned m_G of species from cluster 1 are around 1, indicating that
they are formed after one oxidation step (with NO_3), which is consistent with the expectation
975 for early-generation-products. However, the returned m_G of some species from cluster 1 are
between 1 and 2, e.g., the compound(s) with the formula of $\text{C}_5\text{H}_9\text{NO}_5$ (the largest red marker
in Fig. 11). This suggests that such species may consist of isomers originating from more
than one pathway with different number of oxidation steps.

For species belonging to cluster 2, their m_G are mostly in a range from 1 to 2, but there
980 are also some smaller molecules (mainly C3 and C4 species) with larger m_G , indicating that
such fragmented compounds are formed after multiple oxidation steps. With regard to species
from later-generation clusters, the returned m_G values span a broader range, but there are no
compounds with a generation number larger than 4. In general, most of the high-affiliation
species (from both early- and later-generation) fall in the fast-reacting (large k) area, with a
985 few of exceptions having relatively small k and m_G . These two types of compounds are both
kinetically realistic. However, there are several species with large m_G (around 3) but

relatively small k , e.g., $C_{10}H_{17}N_3O_{15}$ and $C_{10}H_{17}N_3O_{16}$ from cluster 5. This suggests that they are slow-forming products that appear after several oxidation steps, which should be difficult to be formed and thus should be low in signal or even undetectable. In fact, the signals of $C_{10}H_{17}N_3O_{15}$ and $C_{10}H_{17}N_3O_{16}$ are extremely low and noisy at the beginning of reaction, as shown in Fig. S8(u) and Fig. S8(v). Detectable increases in signal of these masses are only observed when the NO_3 exposure was relatively high.



995 **Figure 11.** Fitted effective rate constant (k) and generation number (m_G) of the high-affiliation species of each FCM cluster. The cluster centers and members are denoted by color-coded circles and pentagrams, respectively. The circle area is proportional to the average signal intensity of species over the whole experiment.

To conclude, the kinetic parameters derived from GKP fitting to the clusters are reasonable and well correlated to their chemical properties. Specifically, isoprene products formed in the early stage are larger molecules but less oxidized, with relatively high reactivity, while those formed in the later stage tend to be smaller but highly oxidized and less reactive. Fragmented species are exceptions that have a relatively high oxidation degree and reactivity simultaneously.

1005 3.4 Implications to Isoprene- NO_3 chemistry

As noted previously, one big advantage of FCM is that variables can be affiliated to multiple clusters, which relates to many real-world problems in a more realistic and reasonable way. It

is elaborated in Sect. 3.3 that different FCM clusters have distinct differences in chemical and kinetic properties, potentially representing different chemical processes. Therefore, the clustering distribution of a species gives an insight into its formation mechanism.

Figure 12 shows the cluster apportionment of selected major products formed from isoprene oxidation by NO_3 . Since different FCM clusters represents different types of chemical processes or products that have distinct chemical and kinetic properties, a different distribution indicates different formation pathways of the respective species. According to the general reaction scheme of isoprene with NO_3 (Scheme S1), 1N- and 2N-monomers are expected to be the first- and second-generation products, respectively. The accretion products are supposed to be formed from $\text{RO}_2 + \text{RO}_2$ reaction (Berndt et al., 2018), and thus 2N-dimers are probably originating from self- or cross-reactions of two C5-nitroxy peroxy radicals, while 3N-dimers are most likely produced by cross-reactions of C5-nitroxy peroxy radicals with C5-dinitroxy peroxy radicals (Ng et al., 2008; Wu et al., 2021). Accordingly, 2N- and 3N-dimer should be first- and second-generation products, respectively. Possible permutation scheme for the formation of 2N- and 3N-dimers can be found in Table S1 in the supplement.

The FCM results affirm these suppositions to some extent. For example, 1N-monomer species like $\text{C}_5\text{H}_9\text{NO}_4$ and $\text{C}_5\text{H}_9\text{NO}_5$ are predominant in early-generation clusters (cluster 1 and cluster 2), while 2N-monomers are mostly found in the later-generation clusters (cluster 3 and cluster 4). However, there are some exceptions, such as $\text{C}_5\text{H}_7\text{NO}_6$ and $\text{C}_5\text{H}_7\text{NO}_7$. These two species have entirely different cluster distributions compared to $\text{C}_5\text{H}_7\text{NO}_4$ and $\text{C}_5\text{H}_7\text{NO}_5$, regardless of their similar formula composition. The majority of $\text{C}_5\text{H}_7\text{NO}_6$ and $\text{C}_5\text{H}_7\text{NO}_7$ is apportioned to the second-generation cluster (cluster 3), indicating that $\text{C}_5\text{H}_7\text{NO}_6$ and $\text{C}_5\text{H}_7\text{NO}_7$ are second-generation products, whereas $\text{C}_5\text{H}_7\text{NO}_4$ and $\text{C}_5\text{H}_7\text{NO}_5$ are subsumed in early-generation products. A similar phenomenon is observed between $\text{C}_5\text{H}_9\text{NO}_7$, $\text{C}_5\text{H}_9\text{NO}_4$, and $\text{C}_5\text{H}_9\text{NO}_5$. Another example is the 3N-dimers. In theory, 3N-dimers are supposed to be second-generation products (Table S1), but the FCM outcomes show that different 3N-dimers are formed from different pathways with different generations. For example, $\text{C}_{10}\text{H}_{17}\text{N}_3\text{O}_{12}$, $\text{C}_{10}\text{H}_{17}\text{N}_3\text{O}_{13}$, and $\text{C}_{10}\text{H}_{17}\text{N}_3\text{O}_{14}$ are supposed to be early-generation products based on the FCM results, whereas $\text{C}_{10}\text{H}_{17}\text{N}_3\text{O}_{15}$ and $\text{C}_{10}\text{H}_{17}\text{N}_3\text{O}_{16}$ are supposed to be third- or even later-generation products that have much lower formation rates compared to typical secondary compounds. This implies that the formation mechanisms of 3N-dimers are more complicated than expected. Further investigation is needed to understand distinct behaviors of different 3N-dimers observed in this study.

In terms of 2N-monomers, the clustering results confirm that they are very likely second-generation products, but some species are probably originated from different formation pathways, even though they have the same generation number. As shown in Fig. 12, most fraction of $C_5H_8N_2O_8$ and $C_5H_8N_2O_{10}$ fall into cluster 4, whereas $C_5H_8N_2O_7$, $C_5H_{10}N_2O_8$ and $C_5H_{10}N_2O_9$ are primarily assigned to cluster 3. Cluster 3 and cluster 4 are different in chemical and kinetic properties, as described in Sect. 3.3, which most likely represent two different chemical processes. A similar phenomenon is observed in $C_{10}H_{16}N_2O_{11}$, which has a distinctive distribution compared to other 2N-dimers. This signifies the uniqueness of its formation mechanism.

Although a species can be apportioned to multiple clusters in FCM, most products in this study predominantly belong to one cluster, e.g., $C_5H_9NO_4$ and $C_5H_9NO_6$, suggesting that they were formed predominantly through a single pathway. In contrast, some species are primarily made up of two clusters, such as $C_5H_7NO_5$, $C_5H_9NO_5$, $C_5H_9NO_7$ and $C_{10}H_{17}N_3O_{12}$, which indicates that they are probably comprised of two structural isomers, or that they originate from two different reaction pathways (with different oxidation steps).

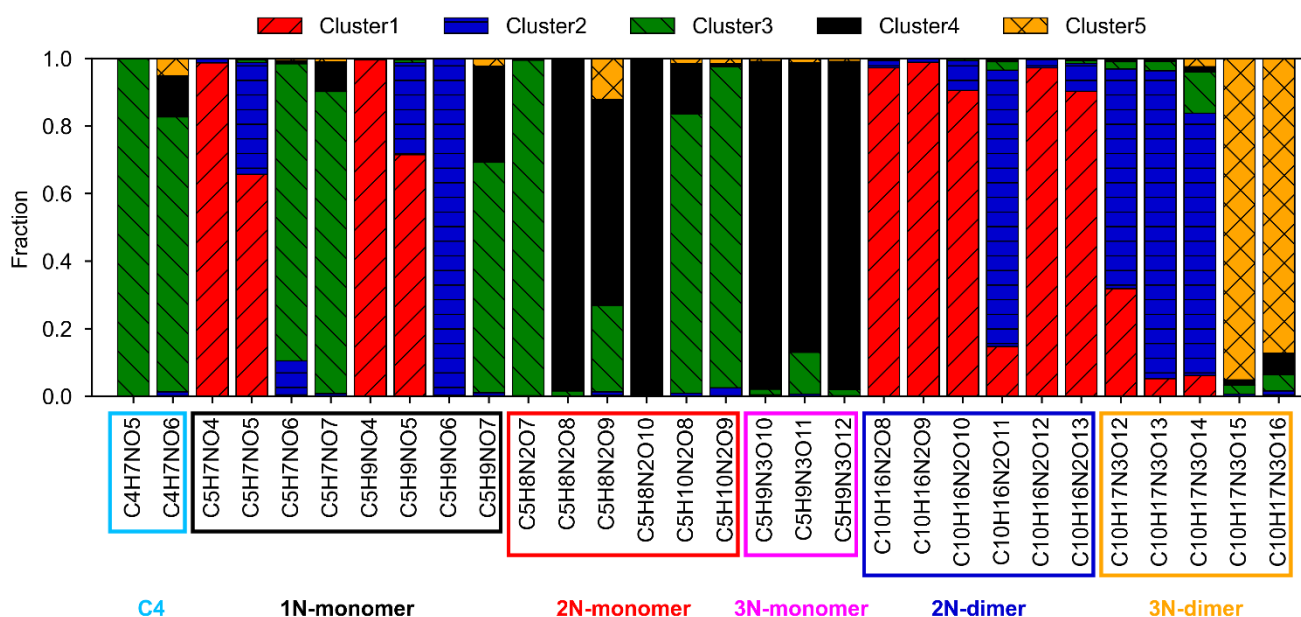


Figure 12. Cluster apportionment of selected major products from the isoprene- NO_3 oxidation system. The colored boxes correspond to different types of products.

All these findings from FCM are valuable and can be used as constraints for mechanism development, especially for less-known species. For example, $C_4H_7NO_5$ is ubiquitous in the atmosphere and contributes significantly to isoprene organonitrates, but it is less investigated (Tsiligiannis et al., 2022). Only a few studies mentioned the formation processes of $C_4H_7NO_5$ in daytime chemistry (Jenkin et al., 2015; Praske et al., 2015; Schwantes et al., 2015;

1065 Wennberg et al., 2018). The formation mechanism of this compound in the nighttime is
unclear yet (Tsiligiannis et al., 2022; Wu et al., 2021). According to the FCM outcomes,
 $C_4H_7NO_5$ is exclusively assigned to cluster 3 (a second-generation cluster), suggesting that
 $C_4H_7NO_5$ is a second-generation product and is mainly originating from a single pathway.
Combining this information together with its molecular composition, we proposed that
1070 $C_4H_7NO_5$ is probably formed via further oxidation of the hydroxy carbonyl ($C_5H_8O_2$) by NO_3 ,
as shown in Scheme S2 in the Supplement (Wu et al., 2021). In a recent publication,
Tsiligiannis et al. (2022) have discussed the sources and fate of $C_4H_7NO_5$ based on both
measurements and modelling results. They suggest that decomposition of $C_5H_8NO_7$ radicals,
nitrated epoxides, or peroxides are also plausible formation pathways for nighttime $C_4H_7NO_5$.
1075 Nonetheless, the fuzzy clustering results suggest that there is only one major formation
channel (or maybe an unknown pathway) for $C_4H_7NO_5$ detected in our system.

4. Conclusions

Recent advances in mass spectrometry, especially the development of CIMS, empowers us to
detect low-volatility vapors in the gas phase directly and largely enhances our understanding
1080 of the formation mechanism of SOA. However, the complex, highly resolved mass spectra
introduce new difficulties for data processing and interpreting. Although different statistical
analysis techniques, such as PMF, PCA, and HCA, have been proposed and widely used to
analyze mass spectrometric data, the application of fuzzy clustering algorithms in analyzing
CIMS data has not yet come into common view.

1085 In this study, we promote adopting the FCM method for the analysis of CIMS data
obtained from complex oxidation systems. Different from hard clustering algorithms, FCM
allows variables to belong to multiple clusters, which is more suitable for overlapping data,
and more reasonable for measurements in atmospheric science.

Several parameters need to be defined before running FCM, such as the number of
1090 clusters, fuzzifier value, and the distance metric used for measuring dissimilarity, which have
an critical effect on clustering outcomes. By using multiple clustering validity indices, the
impacts of these parameters on partition were evaluated, and their optimal values were
determined for our dataset. Furthermore, based on a practical case, we exemplified the
functionalities of FCM in understanding the chemical and kinetic properties of the
1095 investigated system.

Overall, the FCM approach we presented in this work is an applicable and useful tool to analyze mass spectrometric data. It largely simplifies the characterization of an oxidation system by grouping numerous products into a much smaller number of clusters based on their different chemical and kinetic properties. The chemical and kinetic information retained from the clustering outcomes helps to understand the chemical processes involved in the investigated system and can be useful for mechanism development.

Data availability

All data given in figures can be displayed in table or in digital form, including those given in the Supplement. Please send all requests for data to t.mentel@fz-juelich.de and r.wu@fz-juelich.de. The chamber data used in this work are available on the EUROCHAMP database, (<https://data.eurochamp.org/data-access/chamber-experiments/>, EUROCHAMP, 2020) under <https://doi.org/10.25326/JTYK-5V47> (Fuchs et al., 2020).

Competing interests

The authors declare that they have no conflict of interest.

1110 Author contributions

TFM and SRZ designed the study. RW and SK collected CIMS data, and RW did the data analysis. RW and TFM wrote the paper. All co-authors discussed the results and commented on the paper.

Acknowledgement

1115 This work has received funding from the European Research Council (ERC) and European Commission (EC) under the European Union's Horizon 2020 research and innovation program (SARLEP grant agreement No. 681529, and Eurochamp 2020 grant agreement No. 730997). The personnel of the ISOPNO₃ campaign are acknowledged for the help during the campaign.

1120 FORCES!

References

- 1125 Äijälä, M., Heikkinen, L., Fröhlich, R., Canonaco, F., Prévôt, A. S., Junninen, H., Petäjä, T.,
Kulmala, M., Worsnop, D., and Ehn, M.: Resolving anthropogenic aerosol pollution types–
deconvolution and exploratory classification of pollution events, *Atmospheric Chemistry
and Physics*, 17, 3165-3197, 2017.
- 1130 Albrecht, S. R., Novelli, A., Hofzumahaus, A., Kang, S., Baker, Y., Mentel, T., Wahner, A.,
and Fuchs, H.: Measurements of hydroperoxy radicals (HO₂) at atmospheric
concentrations using bromide chemical ionisation mass spectrometry, *Atmospheric
Measurement Techniques*, 12, 891-902, 10.5194/amt-12-891-2019, 2019.
- Arora, J., Khatter, K., and Tushir, M.: Fuzzy c-means clustering strategies: A review of
distance measures, *Software Engineering*, 153-162, 2019.
- 1135 Berndt, T., Scholz, W., Mentler, B., Fischer, L., Herrmann, H., Kulmala, M., and Hansel, A.:
Accretion Product Formation from Self- and Cross-Reactions of RO₂ Radicals in the
Atmosphere, *Angew Chem Int Ed Engl*, 57, 3820-3824, 10.1002/anie.201710989, 2018.
- Bezdek, J. C. and Pal, N. R.: Some new indexes of cluster validity, *IEEE Transactions on
Systems, Man, and Cybernetics, Part B (Cybernetics)*, 28, 301-315, 1998.
- Bezdek, J. C., Ehrlich, R., and Full, W.: FCM: The fuzzy c-means clustering algorithm,
Computers & geosciences, 10, 191-203, 1984.
- 1140 Bianchi, F., Kurten, T., Riva, M., Mohr, C., Rissanen, M. P., Roldin, P., Berndt, T., Crouse,
J. D., Wennberg, P. O., Mentel, T. F., Wildt, J., Junninen, H., Jokinen, T., Kulmala, M.,
Worsnop, D. R., Thornton, J. A., Donahue, N., Kjaergaard, H. G., and Ehn, M.: Highly
Oxygenated Organic Molecules (HOM) from Gas-Phase Autoxidation Involving Peroxy
Radicals: A Key Contributor to Atmospheric Aerosol, *Chem Rev*, 119, 3472-3509,
1145 10.1021/acs.chemrev.8b00395, 2019.
- Bouguessa, M. and Wang, S.-R.: A new efficient validity index for fuzzy clustering,
*Proceedings of 2004 International Conference on Machine Learning and Cybernetics
(IEEE Cat. No. 04EX826)*, 1914-1919.
- Bouguessa, M., Wang, S., and Sun, H.: An objective approach to cluster validation, *Pattern
1150 Recognition Letters*, 27, 1419-1430, 10.1016/j.patrec.2006.01.015, 2006.
- Bozzetti, C., El Haddad, I., Salameh, D., Daellenbach, K. R., Fermo, P., Gonzalez, R.,
Minguillón, M. C., Iinuma, Y., Poulain, L., and Elser, M.: Organic aerosol source

- apportionment by offline-AMS over a full year in Marseille, *Atmospheric Chemistry and Physics*, 17, 8247-8268, 2017.
- 1155 Breitenlechner, M., Fischer, L., Hainer, M., Heinritzi, M., Curtius, J., and Hansel, A.: PTR3: an instrument for studying the lifecycle of reactive organic carbon in the atmosphere, *Analytical chemistry*, 89, 5824-5831, 2017.
- Brown, S. G., Frankel, A., and Hafner, H. R.: Source apportionment of VOCs in the Los Angeles area using positive matrix factorization, *Atmospheric Environment*, 41, 227-237, 1160 2007.
- Buchholz, A., Ylisirniö, A., Huang, W., Mohr, C., Canagaratna, M., Worsnop, D. R., Schobesberger, S., and Virtanen, A.: Deconvolution of FIGAERO-CIMS thermal desorption profiles using positive matrix factorisation to identify chemical and physical processes during particle evaporation, *Atmos. Chem. Phys.*, 20, 7693-7716, 1165 <https://doi.org/10.5194/acp-20-7693-2020>, 2020.
- Campello, R. J. G. B. and Hruschka, E. R.: A fuzzy extension of the silhouette width criterion for cluster analysis, *Fuzzy Sets and Systems*, 157, 2858-2875, 10.1016/j.fss.2006.07.006, 2006.
- Canonaco, F., Crippa, M., Slowik, J. G., Baltensperger, U., and Prévôt, A. S.: SoFi, an IGOR-based interface for the efficient use of the generalized multilinear engine (ME-2) for the 1170 source apportionment: ME-2 application to aerosol mass spectrometer data, *Atmospheric Measurement Techniques*, 6, 3649-3661, 2013.
- Carlsson, P., Vereecken, L., Novelli, A., Bernard, F., Brown, S. S., Brownwood, B., Cho, C., Crowley, J. N., Dewald, P., and Edwards, P. M.: Comparison of isoprene chemical 1175 mechanisms at atmospheric night-time conditions in chamber experiments: Evidence of hydroperoxy aldehydes and epoxy products from NO₃ oxidation, *EGUsphere*, 1-50, 2022.
- Carlton, A. G., Wiedinmyer, C., and Kroll, J. H.: A review of Secondary Organic Aerosol (SOA) formation from isoprene, *Atmos. Chem. Phys.*, 9, 4987-5005, 10.5194/acp-9-4987-2009, 2009.
- 1180 Chen, H.-y., Teng, Y.-g., Wang, J.-s., Song, L.-t., and Zuo, R.: Source apportionment of sediment PAHs in the Pearl River Delta region (China) using nonnegative matrix factorization analysis with effective weighted variance solution, *Science of the total environment*, 444, 401-408, 2013.
- Chen, L.-W. A., Watson, J. G., Chow, J. C., DuBois, D. W., and Herschberger, L.: PM_{2.5} 1185 source apportionment: reconciling receptor models for US nonurban and urban long-term networks, *Journal of the Air & Waste Management Association*, 61, 1204-1217, 2011.

- Chhabra, P., Ng, N., Canagaratna, M., Corrigan, A., Russell, L., Worsnop, D., Flagan, R., and Seinfeld, J.: Elemental composition and oxidation of chamber organic aerosol, *Atmospheric Chemistry and Physics*, 11, 8827-8845, 2011.
- 1190 Crouse, J. D., Nielsen, L. B., Jørgensen, S., Kjaergaard, H. G., and Wennberg, P. O.: Autoxidation of Organic Compounds in the Atmosphere, *The Journal of Physical Chemistry Letters*, 4, 3513-3520, 10.1021/jz4019207, 2013.
- Devarajan, K.: Nonnegative matrix factorization: an analytical and interpretive tool in computational biology, *PLoS computational biology*, 4, e1000029, 2008.
- 1195 Dik, A., Bouroumi, A., and Ettouhami, A.: Weighted distances for fuzzy clustering, *Applied Mathematical Sciences*, 8, 147-156, 2014.
- Donahue, N. M., Kroll, J. H., Pandis, S. N., and Robinson, A. L.: A two-dimensional volatility basis set – Part 2: Diagnostics of organic-aerosol evolution, *Atmos. Chem. Phys.*, 12, 615-634, 2012.
- 1200 Ehn, M., Kleist, E., Junninen, H., Petäjä, T., Lönn, G., Schobesberger, S., Dal Maso, M., Trimborn, A., Kulmala, M., Worsnop, D. R., Wahner, A., Wildt, J., and Mentel, T. F.: Gas phase formation of extremely oxidized pinene reaction products in chamber and ambient air, *Atmospheric Chemistry and Physics*, 12, 5113-5127, 10.5194/acp-12-5113-2012, 2012.
- Ehn, M., Thornton, J. A., Kleist, E., Sipila, M., Junninen, H., Pullinen, I., Springer, M., 1205 Rubach, F., Tillmann, R., Lee, B., Lopez-Hilfiker, F., Andres, S., Acir, I. H., Rissanen, M., Jokinen, T., Schobesberger, S., Kangasluoma, J., Kontkanen, J., Nieminen, T., Kurten, T., Nielsen, L. B., Jørgensen, S., Kjaergaard, H. G., Canagaratna, M., Maso, M. D., Berndt, T., Petaja, T., Wahner, A., Kerminen, V. M., Kulmala, M., Worsnop, D. R., Wildt, J., and Mentel, T. F.: A large source of low-volatility secondary organic aerosol, *Nature*, 506, 1210 476-479, 10.1038/nature13032, 2014.
- Fry, J. L., Brown, S. S., Middlebrook, A. M., Edwards, P. M., Campuzano-Jost, P., Day, D. A., Jimenez, J. L., Allen, H. M., Ryerson, T. B., Pollack, I., Graus, M., Warneke, C., de Gouw, J. A., Brock, C. A., Gilman, J., Lerner, B. M., Dubé, W. P., Liao, J., and Welti, A.: Secondary organic aerosol (SOA) yields from NO₃ radical + isoprene based on nighttime 1215 aircraft power plant plume transects, *Atmos. Chem. Phys.*, 18, 11663-11682, 10.5194/acp-18-11663-2018, 2018.
- Fu, X., Huang, K., Sidiropoulos, N. D., and Ma, W.-K.: Nonnegative matrix factorization for signal and data analytics: Identifiability, algorithms, and applications, *IEEE Signal Process. Mag.*, 36, 59-80, 2019.

- 1220 Fukuyama, Y.: A new method of choosing the number of clusters for the fuzzy c-mean method, *Proc. 5th Fuzzy Syst. Symp.*, 1989, 247-250.
- Gao, X.-B., PEI, J.-h., and XIE, W.-x.: A study of weighting exponent m in a fuzzy c-means algorithm, *ACTA ELECTONICA SINICA*, 28, 80, 2000.
- Gath, I. and Geva, A. B.: Unsupervised optimal fuzzy clustering, *IEEE Transactions on*
 1225 *pattern analysis and machine intelligence*, 11, 773-780, 1989.
- Ghosh, S. and Dubey, S. K.: Comparative analysis of k-means and fuzzy c-means algorithms, *International Journal of Advanced Computer Science and Applications*, 4, 2013.
- Gueorguieva, N., Valova, I., and Georgiev, G.: M&MFCM: fuzzy c-means clustering with mahalanobis and minkowski distance metrics, *Procedia computer science*, 114, 224-233,
 1230 2017.
- Hallquist, M., Wenger, J., Baltensperger, U., Rudich, Y., Simpson, D., Claeys, M., Dommen, J., Donahue, N., George, C., and Goldstein, A.: The formation, properties and impact of secondary organic aerosol: current and emerging issues, *Atmospheric Chemistry and Physics*, 9, 5155-5236, 2009.
- 1235 Hammah, R. and Curran, J.: Fuzzy cluster algorithm for the automatic identification of joint sets, *International Journal of Rock Mechanics and Mining Sciences*, 35, 889-905, 1998.
- Haqiqi, B. N. and Kurniawan, R.: Analisis Perbandingan Metode Fuzzy C-Means Dan Subtractive Fuzzy C-Means, *Media Statistika*, 8, 59-67, 2015.
- Hastie, T., Tibshirani, R., Friedman, J. H., and Friedman, J. H.: *The elements of statistical*
 1240 *learning: data mining, inference, and prediction*, Springer2009.
- Hathaway, R. J. and Bezdek, J. C.: Fuzzy c-means clustering of incomplete data, *IEEE Transactions on Systems, Man, and Cybernetics, Part B (Cybernetics)*, 31, 735-744, 2001.
- Heikkinen, L., Äijälä, M., Daellenbach, K. R., Chen, G., Garmash, O., Aliaga, D., Graeffe, F., Rätty, M., Luoma, K., and Aalto, P.: Eight years of sub-micrometre organic aerosol
 1245 composition data from the boreal forest characterized using a machine-learning approach, *Atmospheric Chemistry and Physics*, 21, 10081-10109, 2021.
- Huang, M., Xia, Z., Wang, H., Zeng, Q., and Wang, Q.: The range of the value for the fuzzifier of the fuzzy c-means algorithm, *Pattern Recognition Letters*, 33, 2280-2284, 2012.
- Hwang, C. and Rhee, F. C.-H.: Uncertain fuzzy clustering: Interval type-2 fuzzy approach to
 1250 c-means, *IEEE Transactions on fuzzy systems*, 15, 107-120, 2007.
- Jenkin, M. E., Young, J. C., and Rickard, A. R.: The MCM v3.3.1 degradation scheme for isoprene, *Atmospheric Chemistry and Physics*, 15, 11433-11459, 10.5194/acp-15-11433-2015, 2015.

- 1255 Jimenez, J. L., Canagaratna, M., Donahue, N., Prevot, A., Zhang, Q., Kroll, J. H., DeCarlo, P. F., Allan, J. D., Coe, H., and Ng, N.: Evolution of organic aerosols in the atmosphere, *science*, 326, 1525-1529, 2009.
- 1260 Jokinen, T., Berndt, T., Makkonen, R., Kerminen, V. M., Junninen, H., Paasonen, P., Stratmann, F., Herrmann, H., Guenther, A. B., Worsnop, D. R., Kulmala, M., Ehn, M., and Sipila, M.: Production of extremely low volatile organic compounds from biogenic emissions: Measured yields and atmospheric implications, *Proc Natl Acad Sci U S A*, 112, 7123-7128, 10.1073/pnas.1423977112, 2015.
- Karl, T., Striednig, M., Graus, M., Hammerle, A., and Wohlfahrt, G.: Urban flux measurements reveal a large pool of oxygenated volatile organic compound emissions, *Proceedings of the National Academy of Sciences*, 115, 1186-1191, 2018.
- 1265 Kaufman, L. and Rousseeuw, P. J.: *Finding groups in data: an introduction to cluster analysis*, John Wiley & Sons 2009.
- 1270 Kirkby, J., Duplissy, J., Sengupta, K., Frege, C., Gordon, H., Williamson, C., Heinritzi, M., Simon, M., Yan, C., Almeida, J., Trostl, J., Nieminen, T., Ortega, I. K., Wagner, R., Adamov, A., Amorim, A., Bernhammer, A. K., Bianchi, F., Breitenlechner, M., Brilke, S., Chen, X., Craven, J., Dias, A., Ehrhart, S., Flagan, R. C., Franchin, A., Fuchs, C., Guida, R., Hakala, J., Hoyle, C. R., Jokinen, T., Junninen, H., Kangasluoma, J., Kim, J., Krapf, M., Kurten, A., Laaksonen, A., Lehtipalo, K., Makhmutov, V., Mathot, S., Molteni, U., Onnela, A., Perakyla, O., Piel, F., Petaja, T., Praplan, A. P., Pringle, K., Rap, A., Richards, N. A., Riipinen, I., Rissanen, M. P., Rondo, L., Sarnela, N., Schobesberger, S., Scott, C. E.,
1275 Seinfeld, J. H., Sipila, M., Steiner, G., Stozhkov, Y., Stratmann, F., Tome, A., Virtanen, A., Vogel, A. L., Wagner, A. C., Wagner, P. E., Weingartner, E., Wimmer, D., Winkler, P. M., Ye, P., Zhang, X., Hansel, A., Dommen, J., Donahue, N. M., Worsnop, D. R., Baltensperger, U., Kulmala, M., Carslaw, K. S., and Curtius, J.: Ion-induced nucleation of pure biogenic particles, *Nature*, 533, 521-526, 10.1038/nature17953, 2016.
- 1280 Koss, A. R., Canagaratna, M. R., Zaytsev, A., Krechmer, J. E., Breitenlechner, M., Nihill, K. J., Lim, C. Y., Rowe, J. C., Roscioli, J. R., and Keutsch, F. N.: Dimensionality-reduction techniques for complex mass spectrometric datasets: application to laboratory atmospheric organic oxidation experiments, *Atmospheric chemistry and physics*, 20, 1021-1041, 2020.
- 1285 Krechmer, J., Lopez-Hilfiker, F., Koss, A., Hutterli, M., Stoerner, C., Deming, B., Kimmel, J., Warneke, C., Holzinger, R., Jayne, J., Worsnop, D., Fuhrer, K., Gonin, M., and de Gouw, J.: Evaluation of a New Reagent-Ion Source and Focusing Ion-Molecule Reactor

- for Use in Proton-Transfer-Reaction Mass Spectrometry, *Anal Chem*, 90, 12011-12018, 10.1021/acs.analchem.8b02641, 2018.
- 1290 Kroll, J. H., Ng, N. L., Murphy, S. M., Flagan, R. C., and Seinfeld, J. H.: Secondary organic aerosol formation from isoprene photooxidation, *Environ. Sci. Technol.*, 40, 1869–1877, <https://doi.org/10.1021/es0524301>, 2006.
- Kryszczuk, K. and Hurley, P.: Estimation of the number of clusters using multiple clustering validity indices, *International workshop on multiple classifier systems*, 114-123,
- 1295 Kwon, S.-H.: Cluster validity index for fuzzy clustering, *Electronics Letters*, 34, 2176-2177, 1998.
- Kwon, S. H., Kim, J., and Son, S. H.: Improved cluster validity index for fuzzy clustering, *Electronics Letters*, 57, 792-794, 2021.
- Lanz, V., Alfarra, M., Baltensperger, U., Buchmann, B., Hueglin, C., and Prévôt, A.: Source apportionment of submicron organic aerosols at an urban site by factor analytical
- 1300 modelling of aerosol mass spectra, *Atmospheric Chemistry and Physics*, 7, 1503-1522, 2007.
- Lanz, V. A., Henne, S., Staehelin, J., Hueglin, C., Vollmer, M. K., Steinbacher, M., Buchmann, B., and Reimann, S.: Statistical analysis of anthropogenic non-methane VOC variability at a European background location (Jungfraujoch, Switzerland), *Atmospheric*
- 1305 *Chemistry and Physics*, 9, 3445-3459, 2009.
- Lanz, V. A., Alfarra, M. R., Baltensperger, U., Buchmann, B., Hueglin, C., Szidat, S., Wehrli, M. N., Wacker, L., Weimer, S., and Caseiro, A.: Source attribution of submicron organic aerosols during wintertime inversions by advanced factor analysis of aerosol mass spectra, *Environmental science & technology*, 42, 214-220, 2008.
- 1310 Lee, D. D. and Seung, H. S.: Learning the parts of objects by non-negative matrix factorization, *Nature*, 401, 788-791, 1999.
- Li, H., Canagaratna, M. R., Riva, M., Rantala, P., Zhang, Y., Thomas, S., Heikkinen, L., Flaud, P.-M., Villenave, E., and Perraudin, E.: Atmospheric organic vapors in two European pine forests measured by a Vocus PTR-TOF: insights into monoterpene and
- 1315 sesquiterpene oxidation processes, *Atmospheric Chemistry and Physics*, 21, 4123-4147, 2021.
- Li, Z., D'Ambro, E. L., Schobesberger, S., Gaston, C. J., Lopez-Hilfiker, F. D., Liu, J., Shilling, J. E., Thornton, J. A., and Cappa, C. D.: A robust clustering algorithm for analysis of composition-dependent organic aerosol thermal desorption measurements, *Atmospheric*
- 1320 *Chemistry and Physics*, 20, 2489-2512, 2020.

- Malley, C. S., Braban, C. F., and Heal, M. R.: The application of hierarchical cluster analysis and non-negative matrix factorization to European atmospheric monitoring site classification, *Atmospheric research*, 138, 30-40, 2014.
- 1325 Ng, N., Kwan, A., Surratt, J., Chan, A., Chhabra, P., Sorooshian, A., Pye, H. O., Crounse, J., Wennberg, P., and Flagan, R.: Secondary organic aerosol (SOA) formation from reaction of isoprene with nitrate radicals (NO₃), *Atmospheric Chemistry and Physics*, 8, 4117–4140, 2008.
- 1330 Nishom, M.: Perbandingan Akurasi Euclidean Distance, Minkowski Distance, dan Manhattan Distance pada Algoritma K-Means Clustering berbasis Chi-Square, *Jurnal Informatika*, 4, 20-24, 2019.
- Ozkan, I. and Turksen, I.: Upper and lower values for the level of fuzziness in FCM, in: *Fuzzy Logic*, Springer, 99-112, 2007.
- Paatero, P.: Least squares formulation of robust non-negative factor analysis, *Chemometrics and intelligent laboratory systems*, 37, 23-35, 1997.
- 1335 Paatero, P. and Tapper, U.: Positive matrix factorization: A non - negative factor model with optimal utilization of error estimates of data values, *Environmetrics*, 5, 111-126, 1994.
- Pal, N. R. and Bezdek, J. C.: On cluster validity for the fuzzy c-means model, *IEEE Transactions on Fuzzy systems*, 3, 370-379, 1995.
- 1340 Pöschl, U.: Atmospheric aerosols: composition, transformation, climate and health effects, *Angewandte Chemie International Edition*, 44, 7520-7540, 2005.
- Praske, E., Crounse, J. D., Bates, K. H., Kurtén, T., Kjaergaard, H. G., and Wennberg, P. O.: Atmospheric fate of methyl vinyl ketone: Peroxy radical reactions with NO and HO₂, *The Journal of Physical Chemistry A*, 119, 4562-4572, 2015.
- 1345 Praske, E., Otkjær, R. V., Crounse, J. D., Hethcox, J. C., Stoltz, B. M., Kjaergaard, H. G., and Wennberg, P. O.: Atmospheric autoxidation is increasingly important in urban and suburban North America, *Proceedings of the National Academy of Sciences*, 115, 64-69, 2018.
- 1350 Priestley, M., Bannan, T. J., Le Breton, M., Worrall, S. D., Kang, S., Pullinen, I., Schmitt, S., Tillmann, R., Kleist, E., Zhao, D., Wildt, J., Garmash, O., Mehra, A., Bacak, A., Shallcross, D. E., Kiendler-Scharr, A., Hallquist, Å. M., Ehn, M., Coe, H., Percival, C. J., Hallquist, M., Mentel, T. F., and McFiggans, G.: Chemical characterisation of benzene oxidation products under high- and low-NO₂ conditions

- using chemical ionisation mass spectrometry, *Atmospheric Chemistry and Physics*, 21, 3473-3490, 10.5194/acp-21-3473-2021, 2021.
- 1355 Pullinen, I., Schmitt, S., Kang, S., Sarrafzadeh, M., Schlag, P., Andres, S., Kleist, E., Mentel, T. F., Rohrer, F., and Springer, M.: Impact of NO_x on secondary organic aerosol (SOA) formation from α -pinene and β -pinene photooxidation: the role of highly oxygenated organic nitrates, *Atmospheric chemistry and physics*, 20, 10125-10147, 2020.
- Rawashdeh, M. and Ralescu, A. L.: Fuzzy Cluster Validity with Generalized Silhouettes, 1360 *Midwest Artificial Intelligence and Cognitive Science Conference*, 2012.
- Reff, A., Eberly, S. I., and Bhave, P. V.: Receptor modeling of ambient particulate matter data using positive matrix factorization: review of existing methods, *Journal of the Air & Waste Management Association*, 57, 146-154, 2007.
- Ren, M., Liu, P., Wang, Z., and Yi, J.: A self-adaptive fuzzy c-means algorithm for 1365 determining the optimal number of clusters, *Computational intelligence and neuroscience*, 2016, 2016.
- Rohrer, F., Bohn, B., Brauers, T., Brüning, D., Johnen, F. J., Wahner, A., and Kleffmann, J.: Characterisation of the photolytic HONO-source in the atmosphere simulation chamber SAPHIR, *Atmospheric Chemistry and Physics*, 5, 2189-2201, 10.5194/acp-5-2189-2005, 1370 2005.
- Rollins, A. W., Kiendler-Scharr, A., Fry, J., Brauers, T., Brown, S. S., Dorn, H.-P., Dubé, W. P., Fuchs, H., Mensah, A., and Mentel, T.: Isoprene oxidation by nitrate radical: alkyl nitrate and secondary organic aerosol yields, *Atmos. Chem. Phys.*, 9, 6685–6703, 10.5194/acp-9-6685-2009, 2009.
- 1375 Rosati, B., Teiwes, R., Kristensen, K., Bossi, R., Skov, H., Glasius, M., Pedersen, H. B., and Bilde, M.: Factor analysis of chemical ionization experiments: Numerical simulations and an experimental case study of the ozonolysis of α -pinene using a PTR-ToF-MS, *Atmospheric Environment*, 199, 15-31, 2019.
- Rousseeuw, P. J.: Silhouettes: a graphical aid to the interpretation and validation of cluster 1380 analysis, *Journal of computational and applied mathematics*, 20, 53-65, 1987
- Schwämmle, V. and Jensen, O. N.: A simple and fast method to determine the parameters for fuzzy c-means cluster analysis, *Bioinformatics*, 26, 2841-2848, 2010.
- Schwantes, R. H., Teng, A. P., Nguyen, T. B., Coggon, M. M., Crouse, J. D., St Clair, J. M., Zhang, X., Schilling, K. A., Seinfeld, J. H., and Wennberg, P. O.: Isoprene NO₃ Oxidation 1385 Products from the RO₂ + HO₂ Pathway, *J Phys Chem A*, 119, 10158-10171, 10.1021/acs.jpca.5b06355, 2015.

- Shrivastava, M., Cappa, C. D., Fan, J., Goldstein, A. H., Guenther, A. B., Jimenez, J. L., Kuang, C., Laskin, A., Martin, S. T., Ng, N. L., Petaja, T., Pierce, J. R., Rasch, P. J., Roldin, P., Seinfeld, J. H., Shilling, J., Smith, J. N., Thornton, J. A., Volkamer, R., Wang, J., Worsnop, D. R., Zaveri, R. A., Zelenyuk, A., and Zhang, Q.: Recent advances in understanding secondary organic aerosol: Implications for global climate forcing, *Reviews of Geophysics*, 55, 509-559, 10.1002/2016rg000540, 2017.
- 1390
- Simovici, D. A. and Jaroszewicz, S.: An axiomatization of partition entropy, *IEEE Transactions on Information Theory*, 48, 2138-2142, 2002.
- 1395
- Singh, A., Agarwal, J., and Rana, A.: Performance measure of similis and fp-growth algorithm, *International Journal of Computer Applications*, 62, 2013.
- Sofowote, U. M., McCarry, B. E., and Marvin, C. H.: Source apportionment of PAH in Hamilton Harbour suspended sediments: comparison of two factor analysis methods, *Environmental science & technology*, 42, 6007-6014, 2008.
- 1400
- Song, K., Guo, S., Wang, H., Yu, Y., Wang, H., Tang, R., Xia, S., Gong, Y., Wan, Z., and Lv, D.: Measurement report: Online measurement of gas-phase nitrated phenols utilizing a CI-LToF-MS: primary sources and secondary formation, *Atmospheric Chemistry and Physics*, 21, 7917-7932, 2021.
- 1405
- Spracklen, D., Jimenez, J., Carslaw, K., Worsnop, D., Evans, M., Mann, G., Zhang, Q., Canagaratna, M., Allan, J., and Coe, H.: Aerosol mass spectrometer constraint on the global secondary organic aerosol budget, *Atmospheric Chemistry and Physics*, 11, 12109-12136, 2011.
- 1410
- Stark, H., Yatavelli, R. L. N., Thompson, S. L., Kimmel, J. R., Cubison, M. J., Chhabra, P. S., Canagaratna, M. R., Jayne, J. T., Worsnop, D. R., and Jimenez, J. L.: Methods to extract molecular and bulk chemical information from series of complex mass spectra with limited mass resolution, *International Journal of Mass Spectrometry*, 389, 26-38, 10.1016/j.ijms.2015.08.011, 2015.
- 1415
- Subbalakshmi, C., Krishna, G. R., Rao, S. K. M., and Rao, P. V.: A method to find optimum number of clusters based on fuzzy silhouette on dynamic data set, *Procedia Computer Science*, 46, 346-353, 2015.
- Surratt, J. D., Lin, Y.-H., Arashiro, M., Vizuete, W. G., Zhang, Z., Gold, A., Jaspers, I., and Fry, R. C.: Understanding the early biological effects of isoprene-derived particulate matter enhanced by anthropogenic pollutants, *Research Reports: Health Effects Institute*, 2019, 2019.

- 1420 Tsiligiannis, E., Wu, R., Lee, B. H., Salvador, C. M., Priestley, M., Carlsson, P. T., Kang, S.,
Novelli, A., Vereecken, L., and Fuchs, H.: A four carbon organonitrate as a significant
product of secondary isoprene chemistry, *Geophysical research letters*, 49,
e2021GL097366, 2022.
- Ulbrich, I., Canagaratna, M., Zhang, Q., Worsnop, D., and Jimenez, J.: Interpretation of
1425 organic components from Positive Matrix Factorization of aerosol mass spectrometric data,
Atmospheric Chemistry and Physics, 9, 2891-2918, 2009.
- Vélez-Falconí, M., Marín, J., Jiménez, S., and Guachi-Guachi, L.: Comparative Study of
Distance Measures for the Fuzzy C-means and K-means Non-Supervised Methods Applied
to Image Segmentation, *ICAI Workshops*, 1-14,
- 1430 Vereecken, L., Carlsson, P., Novelli, A., Bernard, F., Brown, S., Cho, C., Crowley, J., Fuchs,
H., Mellouki, W., and Reimer, D.: Theoretical and experimental study of peroxy and
alkoxy radicals in the NO₃-initiated oxidation of isoprene, *Physical Chemistry Chemical
Physics*, 23, 5496-5515, 2021.
- Vlasenko, A., Slowik, J., Bottenheim, J., Brickell, P., Chang, R. W., Macdonald, A., Shantz,
1435 N., Sjostedt, S., Wiebe, H., and Leaitch, W.: Measurements of VOCs by proton transfer
reaction mass spectrometry at a rural Ontario site: Sources and correlation to aerosol
composition, *Journal of Geophysical Research: Atmospheres*, 114, 2009.
- Wang, H., Wang, J., and Wang, G.: Combination evaluation method of fuzzy c-mean
clustering validity based on hybrid weighted strategy, *IEEE Access*, 9, 27239-27261, 2021.
- 1440 Wennberg, P. O., Bates, K. H., Crouse, J. D., Dodson, L. G., McVay, R. C., Mertens, L. A.,
Nguyen, T. B., Praske, E., Schwantes, R. H., and Smarte, M. D.: Gas-phase reactions of
isoprene and its major oxidation products, *Chemical reviews*, 118, 3337-3390, 2018.
- Wold, S., Esbensen, K., and Geladi, P.: Principal component analysis, *Chemometrics and
intelligent laboratory systems*, 2, 37-52, 1987.
- 1445 Wu, K.-L.: Analysis of parameter selections for fuzzy c-means, *Pattern Recognition*, 45, 407-
415, 2012.
- Wu, R., Vereecken, L., Tsiligiannis, E., Kang, S., Albrecht, S. R., Hantschke, L., Zhao, D.,
Novelli, A., Fuchs, H., Tillmann, R., Hohaus, T., Carlsson, P. T. M., Shenolikar, J.,
Bernard, F., Crowley, J. N., Fry, J. L., Brownwood, B., Thornton, J. A., Brown, S. S.,
1450 Kiendler-Scharr, A., Wahner, A., Hallquist, M., and Mentel, T. F.: Molecular composition
and volatility of multi-generation products formed from isoprene oxidation by nitrate
radical, *Atmospheric Chemistry and Physics*, 21, 10799-10824, 10.5194/acp-21-10799-
2021, 2021.

- Wyche, K., Monks, P. S., Smallbone, K., Hamilton, J., Alfarra, M., Rickard, A., McFiggans, G. B., Jenkin, M., Bloss, W., and Ryan, A. C.: Mapping gas-phase organic reactivity and concomitant secondary organic aerosol formation: chemometric dimension reduction techniques for the deconvolution of complex atmospheric data sets, *Atmospheric Chemistry and Physics*, 15, 8077-8100, 2015.
- Xie, M., Lu, X., Ding, F., Cui, W., Zhang, Y., and Feng, W.: Evaluating the influence of constant source profile presumption on PMF analysis of PM_{2.5} by comparing long- and short-term hourly observation-based modeling, *Environmental Pollution*, 314, 120273, 2022.
- Xie, X. L. and Beni, G.: A validity measure for fuzzy clustering, *IEEE Transactions on Pattern Analysis & Machine Intelligence*, 13, 841-847, 1991.
- Xu, Z., Nie, W., Liu, Y., Sun, P., Huang, D., Yan, C., Krechmer, J., Ye, P., Xu, Z., and Qi, X.: Multifunctional products of isoprene oxidation in polluted atmosphere and their contribution to SOA, *Geophysical Research Letters*, 48, e2020GL089276, 2021.
- Yan, C., Nie, W., Äijälä, M., Rissanen, M. P., Canagaratna, M. R., Massoli, P., Junninen, H., Jokinen, T., Sarnela, N., Häme, S. A. K., Schobesberger, S., Canonaco, F., Yao, L., Prévôt, A. S. H., Petäjä, T., Kulmala, M., Sipilä, M., Worsnop, D. R., and Ehn, M.: Source characterization of highly oxidized multifunctional compounds in a boreal forest environment using positive matrix factorization, *Atmospheric Chemistry and Physics*, 16, 12715-12731, 10.5194/acp-16-12715-2016, 2016.
- Yang, M. S., Convergence Properties of the Generalized Fuzzy C-Means Clustering Algorithms. *Comput Math Appl* 1993, 25 (12), 3-11.
- Yu, J., Cheng, Q., and Huang, H.: Analysis of the weighting exponent in the FCM, *IEEE Transactions on Systems, Man, and Cybernetics, Part B (Cybernetics)*, 34, 634-639, 2004.
- Yuan, B., Shao, M., De Gouw, J., Parrish, D. D., Lu, S., Wang, M., Zeng, L., Zhang, Q., Song, Y., and Zhang, J.: Volatile organic compounds (VOCs) in urban air: How chemistry affects the interpretation of positive matrix factorization (PMF) analysis, *Journal of Geophysical Research: Atmospheres*, 117, 2012.
- Zadeh, L. A.: Fuzzy sets, *Information and control*, 8, 338-353, 1965.
- Zaytsev, A., Koss, A. R., Breitenlechner, M., Krechmer, J. E., Nihill, K. J., Lim, C. Y., Rowe, J. C., Cox, J. L., Moss, J., Roscioli, J. R., Canagaratna, M. R., Worsnop, D. R., Kroll, J. H., and Keutsch, F. N.: Mechanistic Study of Formation of Ring-retaining and Ring-opening Products from Oxidation of Aromatic Compounds under Urban Atmospheric Conditions, *Atmospheric Chemistry and Physics Discussions*, 1-24, 10.5194/acp-2019-666, 2019.

- Zhang, Q., Alfarra, M. R., Worsnop, D. R., Allan, J. D., Coe, H., Canagaratna, M. R., and Jimenez, J. L.: Deconvolution and quantification of hydrocarbon-like and oxygenated organic aerosols based on aerosol mass spectrometry, *Environmental science & technology*, 39, 4938-4952, 2005.
- 1490 Zhang, Q., Jimenez, J. L., Canagaratna, M. R., Ulbrich, I. M., Ng, N. L., Worsnop, D. R., and Sun, Y.: Understanding atmospheric organic aerosols via factor analysis of aerosol mass spectrometry: a review, *Analytical and bioanalytical chemistry*, 401, 3045-3067, 2011.
- 1495 Zhang, Q., Jimenez, J. L., Canagaratna, M., Allan, J., Coe, H., Ulbrich, I., Alfarra, M., Takami, A., Middlebrook, A., and Sun, Y.: Ubiquity and dominance of oxygenated species in organic aerosols in anthropogenically - influenced Northern Hemisphere midlatitudes, *Geophysical Research Letters*, 34, 2007.
- Zhang, Y., Peräkylä, O., Yan, C., Heikkinen, L., Äijälä, M., Daellenbach, K. R., Zha, Q., Riva, M., Garmash, O., Junninen, H., Paatero, P., Worsnop, D., and Ehn, M.: A Novel Approach for Simple Statistical Analysis of High-Resolution Mass Spectra, *Atmospheric Measurement Techniques Discussions*, 1-32, 10.5194/amt-2019-59, 2019.
- 1500 Zhou, K., Fu, C., and Yang, S.: Fuzziness parameter selection in fuzzy c-means: the perspective of cluster validation, *Science China Information Sciences*, 57, 1-8, 2014.
- 1505 Zhou, Y. and Zhuang, X.: Kinetic analysis of sequential multistep reactions, *The Journal of Physical Chemistry B*, 111, 13600-13610, 2007.
- Ziemann, P. J. and Atkinson, R.: Kinetics, products, and mechanisms of secondary organic aerosol formation, *Chem Soc Rev*, 41, 6582-6605, 10.1039/c2cs35122f, 2012.